Abrupt changes of intermediate water properties on the northeastern slope of the Bering Sea during the last glacial and deglacial period

Stephan F. Rella,[1] Ryuji Tada,[1] Kana Nagashima,[2] Minoru Ikehara,[3] Takuya Itaki,[4] Ken'ichi Ohkushi,[5] Tatsuhiko Sakamoto,[6] Naomi Harada,[2] and Masao Uchida[7]

Received 18 July 2011; revised 20 May 2012; accepted 29 May 2012; published 11 July 2012.

[1] Millennial-scale variability in the behavior of North Pacific Intermediate Water during the last glacial and deglacial period, and its association with Dansgaard-Oeschger (D-O) cycles and Heinrich events, are examined based on benthic foraminiferal oxygen and carbon isotopes ($\delta^{18}O_{bf}$ and $\delta^{13}C_{bf}$) and $\%CaCO_3$ using a sediment core recovered from the northeastern slope of the Bering Sea. A suite of positive $\delta^{18}O_{bf}$ excursions at intermediate depths of the Bering Sea, which seem at least in part associated with increases in the $\delta^{18}O_{bf}$ gradients between the Bering and Okhotsk Seas, suggest the Bering Sea as a proximate source of intermediate water during several severe stadial episodes in the last glacial and deglacial period. Absence of such $\delta^{18}O_{bf}$ gradients during periods of high surface productivity in the Bering and Okhotsk Seas, which we correlate to D-O interstadials, suggests a reduction in intermediate water production in the Bering Sea and subsequent introduction of nutrient-rich deep waters from the North Pacific into intermediate depths of the Bering Sea. We argue that a reorganization of atmospheric circulation in the high-latitude North Pacific during severe cold episodes in the last glacial and deglacial period created favorable conditions for brine rejection in the northeastern Bering Sea. The resulting salinity increase in the cold surface waters could have initiated intermediate (and deep) water formation that spread out to the North Pacific.

Citation: Rella, S. F., R. Tada, K. Nagashima, M. Ikehara, T. Itaki, K. Ohkushi, T. Sakamoto, N. Harada, and M. Uchida (2012), Abrupt changes of intermediate water properties on the northeastern slope of the Bering Sea during the last glacial and deglacial period, *Paleoceanography*, *27*, PA3203, doi:10.1029/2011PA002205.

1. Introduction

[2] While variability of deep and intermediate water circulation in the North Atlantic is well documented for the last glacial and deglacial period [e.g., *Sarnthein et al.*, 2000; *Rahmstorf*, 2002], it is still poorly understood in the North Pacific during that time due to the shallow lysocline that limits paleoceanographic investigations to bathymetric highs and the continental margins with water depths shallower than ca. 2000 m [e.g., *Farrell and Prell*, 1989]. In the modern North Pacific, deep water formation is absent because of low surface salinity that results from excess precipitation over evaporation in the area [e.g., *Warren*, 1983]. However, presence of intermediate water in the North Pacific is evident from a well-defined salinity minimum in the subtropical North Pacific at depths of approximately 300 to 800 m [e.g., *Sverdrup et al.*, 1942; *Reid*, 1965; *Talley*, 1991, 1993; *Yasuda*, 1997], which is called North Pacific Intermediate Water (NPIW). One major modern source area of NPIW is the northern Okhotsk Sea [e.g., *Yasuda*, 1997; *Shcherbina et al.*, 2003], where the formation of Okhotsk Sea Intermediate Water, a precursor of NPIW, is tightly coupled to northwesterly winds that dominate during winter and create polynyas (ice-free zones) in seasonal sea-ice [e.g., *Shcherbina et al.*, 2003; *Katsuki et al.*, 2010].

[3] Knowledge about NPIW formation and its extent is crucial to assess its CO_2 storage capability and the meridional heat transport, which are important components of the global climate system [e.g., *Levitus et al.*, 2000; *Otsuki et al.*, 2003]. During the last glacial period, intermediate water ventilation in the North Pacific apparently reached as

[1]Department of Earth and Planetary Science, University of Tokyo, Tokyo, Japan.
[2]Institute of Observational Research for Global Change, Japan Agency for Marine-Earth Science and Technology, Yokosuka, Japan.
[3]Center for Advanced Marine Core Research, Kochi University, Nankoku, Japan.
[4]Institute of Geology and Geoinformation, AIST, Geological Survey of Japan, Tsukuba, Japan.
[5]Department of Science of Human Environment, Graduate School of Human Development and Environment, Kobe University, Kobe, Japan.
[6]Institute for Research on Earth Evolution, Japan Agency for Marine-Earth Science and Technology, Yokosuka, Japan.
[7]Environmental Chemistry Division, National Institute for Environmental Studies, Tsukuba, Japan.

Corresponding author: S. F. Rella, Department of Earth and Planetary Science, University of Tokyo, 7-3-1 Hongo, Bunkyo-ku, Tokyo 113-0033, Japan. (stephanrella@gmail.com)

0883-8305/12/2011PA002205

deep as ~3000 m based on epifaunal benthic $\delta^{13}C$ [*Duplessy et al.*, 1988; *Matsumoto et al.*, 2002] and NPIW is interpreted to have extended far south to the California margin during D-O stadial periods (DOS) of the last glacial and deglacial period, while it shrank or was absent during D-O interstadial periods (DOIS) [e.g., *Keigwin and Jones*, 1990; *Behl and Kennett*, 1996; *Tada et al.*, 2000; *Hendy and Pedersen*, 2005; *Okazaki et al.*, 2010]. However, because these sites are far from the source regions of NPIW, the observed changes in oxygenation level at intermediate depths [e.g., *Behl and Kennett*, 1996] may not necessarily represent variation in NPIW intensity [*Hendy et al.*, 2004; *Ortiz et al.*, 2004; *McKay et al.*, 2005; *Dean*, 2007]. *Kim and Park* [2008] advocated a source of NPIW in the northern marginal seas of the North Pacific during the last glacial period based on their coupled ocean-atmosphere model. *Ohkushi et al.* [2003] hypothesized glacial NPIW production in the Bering Sea based on distribution patterns of radiolarian assemblages in the Bering and Okhotsk Seas. However, no quantitative data with sufficiently high time resolution has been presented so far on the possibility of intermediate water formation and the mode of its formation in the Bering Sea during the last glacial and deglacial period.

[4] In this study, we examine millennial-scale variability of NPIW and its association with abrupt climatic changes such as D-O cycles during the last glacial period, and Bølling/Allerød (B/A) and Younger Dryas (YD) during the deglacial period. We explore the possibility of the Bering Sea as a locus of NPIW formation by examining oxygen and carbon isotopes of benthic foraminifera (hereafter denoted $\delta^{18}O_{bf}$ and $\delta^{13}C_{bf}$) to infer changes in intermediate water temperature/salinity and oxygenation/ventilation, respectively, using a piston core obtained from the northeastern slope of the Bering Sea. Because $\delta^{18}O_{bf}$ are expected to be higher in the source area of NPIW, we also attempt to estimate the direction of lateral advection and the proximal source of NPIW by comparing $\delta^{18}O_{bf}$ at intermediate depths between the Bering and Okhotsk Seas. In addition, we use % $CaCO_3$ to examine the relationship of surface productivity with intermediate water properties in association with abrupt climatic changes.

2. Oceanographic Setting

[5] The Bering Sea, surrounded by Eastern Siberia and Western Alaska to its north and the Aleutian and the Kommander Islands to its south, is the third largest marginal sea in the world with an area of ca. 2.3×10^6 km^2 [*Hood*, 1983]. A more than 400 km wide and <200 m deep continental shelf (Bering Shelf) occupies the northeastern half of the Bering Sea, while a vast deep basin of ~3900 m depth, called the Aleutian Basin, dominates the southwestern half. A NW-SE running continental slope separates the Bering Shelf and the Aleutian Basin. Two large topographic highs (<2000 m), the Shirshov and Bowers Ridges, extend ca. 500 km into the basin from the north and south, respectively (Figure 1).

[6] Surface waters in the Bering Sea largely originate from the westward flowing Alaskan Current entering through passes between the Aleutian Islands with the largest inflow occurring through the Near Strait [*Favorite et al.*, 1976; *Reed and Stabeno*, 1999] (Figure 1). A cyclonic gyre dominates the surface current regime over the deep basin. The northeastern component of the gyre (along the shelf break), the so-called Bering Slope Current (BSC), feeds in part the southwestward directed Kamchatka Current, the most significant outflow to the North Pacific, and the northeastward directed Anadyr Current that contributes 1/3 of outflowing waters to the Arctic Ocean. The remaining 2/3 of outflowing waters originate from the dominantly northward flowing currents over the Bering Shelf [e.g., *Springer et al.*, 1996]. Deep water exchange between the Bering Sea and the North Pacific occurs through the Kamchatka Strait (~4000 m sill depth) and the Near Strait (~2000 m sill depth). The present deep waters in the Aleutian Basin are most likely derived from the North Pacific Ocean [e.g., *Roden*, 1995; *Emile-Geay et al.*, 2003], although weak recent ventilation in the eastern part of the deep Aleutian Basin has been suggested [*Warner and Roden*, 1995].

[7] Due to delivery of nutrients to the surface waters through upwelling of deep waters and melting of winter ice, the Bering Sea is also characterized by high primary productivity, in particular along the northeastern continental slope known as the Bering Sea Green Belt [*Springer et al.*, 1996]. In the Aleutian Basin, summer insolation warms the upper 30 m of the water column, which is rich in oxygen and low in salinity and nutrients [*Roden*, 1995]. Below the surface layer, a 100 to 150 m thick temperature minimum layer is present, which is likely a remnant of winter convection [*Roden*, 1995]. The halo-, nutri- and oxyclines are found between 150 and 450 m depth. While salinity and density increase uniformly with depth, oxygen minimum and associated nutrient maximum layers are centered at approximately 900 m depth. Vertical profiles of temperature and salinity in the upper 500 m of the water column become almost constant during winter due to severe wind stress that mixes water to depths [*Ohtani et al.*, 1972; *Takahashi*, 2005].

3. Sea Ice Conditions in the Bering Sea and Their Relation to Atmospheric Circulation

[8] At present, the winter sea ice edge in the Bering Sea is situated approximately at the shelf break. Polynyas are common features within the area covered by sea ice and can produce open water for days to weeks [*Roden*, 1995]. Polynya formation in the Bering Sea is related to the direction of storm tracks. For example, southerly winds can drive sea ice northward and close the polynya growth regions [*Rodionov et al.*, 2007]. During anomalously cold winters, on the other hand, the Aleutian Low is displaced eastward of its normal position leading to more northerly winds and sea ice extending farther south [*Rogers*, 1981; *Luchin et al.*, 2002], which is favorable for enhanced polynya formation. Based on the NCEP/NCAR reanalysis data for the period from 1950 to 2003, *Rodionov et al.* [2007] showed that the coldest years in the Bering Sea are associated with anticyclonic circulation driven by intense high pressure cells dominating over northeastern Siberia and cyclone tracks typically running across the North Pacific just to the south of

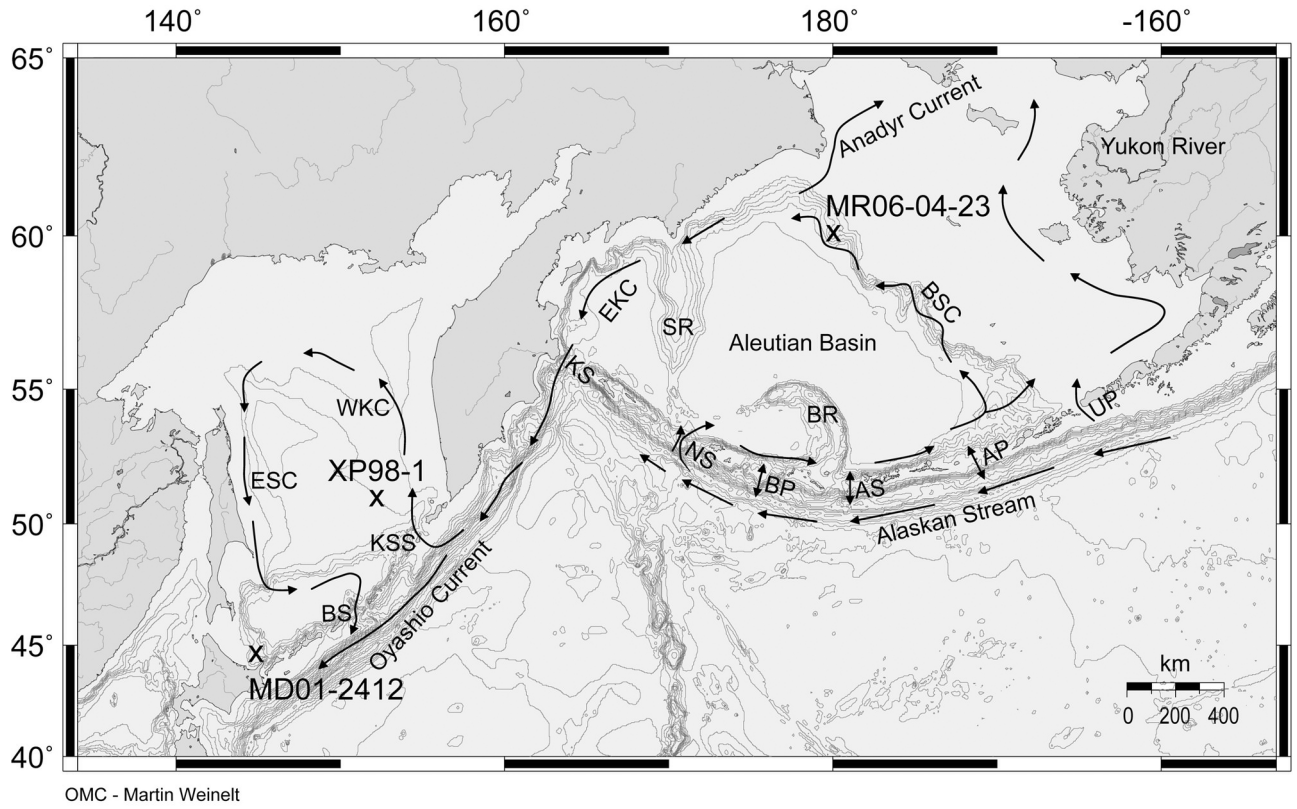

Figure 1. Bathymetric map showing the location of sites cited in this study. Also shown are surface current systems and passes and straits through the Aleutian Islands. SR = Shirshov Ridge, BR = Bowers Ridge, BSC = Bering Slope Current, EKC = East Kamchatka Current, WKC = West Kamchatka Current, ESC = East Sakhalin Current, NS = Near Strait, BP = Buldir Pass, AS = Amchitka Strait, AP = Amutka Pass, UP = Unimak Pass, KSS = Kruzenshtern Strait, BS = Bussol Strait.

the Aleutian Islands. Vigorous air-sea exchange associated with cold air outbreaks and ice formation in areas of polynyas can locally increase surface water salinity up to 35‰ [*Schumacher et al.*, 1983]. Consequently, dense waters may form, contributing to the cold halocline layer in the Aleutian Basin [*Cavalieri and Martin*, 1994].

4. Onboard Sample Preparation

[9] Piston core PC-23A was retrieved in summer 2006 from the upper slope of the northeastern part of the Bering Sea (60°09.52′N, 179°27.82′W) at a water depth of 1002 m during cruise MR06–04 Leg 2 by R/V *Mirai* (MR06–04 cruise report). The recovered core was immediately cut into 1 m long sections, which were left for 24 h, cut horizontally into halves and submitted to routine analyses. Sections were stored in a refrigerator until onboard sampling. Five to ten conventional smear slide analyses were conducted per meter of core during visual core description. Samples for X-ray guide tube micro-scanner (XGT) and soft X-ray radiography analyses were taken as thin slabs in plastic cases of 20 (length) × 2.5 (width) × 0.7 (depth) cm in size. Slab samples were taken continuously throughout the core and were immediately vacuum sealed and double packed to prevent air exchange. Samples used for isotope and ^{14}C analyses of foraminifera and XRF analysis were sub-sampled at 2 cm intervals and double packed in bags. All samples were stored in a refrigerator onboard and then at the University of Tokyo at temperatures of 5°C for 5 to 11 months before analyses.

5. Analytical Methods

5.1. Soft X-ray Analysis

[10] Soft X-ray photographs were taken for all slab samples onboard using a SOFTEX PRO-TEST 150 to examine sedimentary structures and microstructures. Voltages ranging from 40–50 kVp, currents from 2 to 3 mA and irradiation time from 150 to 200 s were used to optimize photographic conditions.

5.2. XGT Analysis

[11] To characterize millennial-scale changes of sediment composition that may reflect changes in surface and/or intermediate water properties, a high resolution analysis of major elements was conducted using an X-ray micro-scanner (Horiba XGT-2700, hereafter designated as XGT), which is capable of continuous high resolution quantitative analysis of major elements [*Koshikawa et al.*, 2003; *Kido et al.*, 2006]. XGT is equipped with a Rh target and an

X-ray guide tube of 100 μm in diameter. A tube voltage of 50 kV, tube current of 1 mA, scanning time of 100 s and scanning area of 1.25 × 1.25 cm were adopted following *Koshikawa et al.* [2003]. We followed the procedures of *Kido et al.* [2006] that make corrections for absorption effects of Mylar film, thin water film and interstitial water to obtain X-ray fluorescence (XRF) intensities for Al, Si, K, Ca, Ti and Fe that are proportional to their contents and can be used for quantitative estimation. In this study, we use $\%Al_2O_3$ and %CaO determined by XGT, which show a good correlation to $\%Al_2O_3$ (r^2 = 0.62) and %CaO (r^2 = 0.8) determined by conventional quantitative XRF.

5.3. Conventional X-Ray Fluorescence Analysis

[12] Conventional XRF analysis was conducted for 102 selected samples to determine major element concentrations of ten elements including Al_2O_3, SiO_2, K_2O, CaO, TiO_2 and Fe_2O_3, which are used to calibrate XRF peak intensities determined by XGT to major element contents. The preparation of glass beads is based on the method described in *Yoshida and Takahashi* [1997]. Measurements were carried out on the glass beads using an XRF spectrometer Phillips Model PW 1480 equipped with a Rh tube at an acceleration voltage of 50 kV and a current of 50 mA at the Department of Earth and Planetary Science, University of Tokyo. The analytical precisions (±sigma %: relative error) were within ±1.3%, ±0.7%, ±3.9%, ±2.9%, ±1.2%, and ±2.0% for Al_2O_3, SiO_2, K_2O, CaO, TiO_2 and Fe_2O_3, respectively [*Yoshida and Takahashi*, 1997]. $\%CaCO_3$ was estimated based on the $CaCO_3$/CaO atomic weight ratio of 100/56. The percentage of biogenic $CaCO_3$ was estimated from total $CaCO_3$ using the equation

$$\%CaCO_{3\ biogenic}(XRF) = \%CaCO_{3\ total}(XRF) - (CaCO_3/Al_2O_3)_{detrital} \times \%Al_2O_3(XRF) \quad (1)$$

$\%CaCO_{3\ total}$ measured by conventional XRF and biogenic $\%CaCO_3$ measured at a similar resolution using a coloumbmeter by *Kim et al.* [2008] show a good correlation (r^2 = 0.86) suggesting that detrital $CaCO_3$ was relatively constant over time at ∼2.8% judging from the intercept of the regression line with the $\%CaCO_{3\ total}$ axis. By applying the average content of Al_2O_3 (∼14.4%) in PC-23A, detrital $CaCO_3/Al_2O_3$ is ∼0.19. We accordingly estimate the contribution of biogenic $CaCO_3$ in total $CaCO_3$ measured by XGT using the equation

$$\%CaCO_{3\ biogenic}(XGT) = \%CaCO_{3\ total}(XGT) - 0.19 \times \%Al_2O_3(XGT) \quad (2)$$

Hereafter, the term $\%CaCO_3$ refers to $\%CaCO_{3\ biogenic}$ (XGT).

5.4. Oxygen and Carbon Isotope Analyses of Benthic Foraminifera

[13] We conducted $\delta^{18}O_{bf}$ and $\delta^{13}C_{bf}$ analyses of benthic foraminifera *Uvigerina akitaensis* and *Buliminella tenuata* from PC-23A in order to reconstruct temporal changes in intermediate water mass properties such as temperature, salinity, and the degree of organic matter decomposition within the intermediate water and surface sediment. Samples were selected at 4 to 14 cm intervals throughout the core (using ∼15 g of sediments per sample). Between 1 and 15 specimens of benthic foraminifera *U. akitaensis* and *B. tenuata* (if available a minimum of 7 specimens for *U. akitaensis* and 10 specimens for *B. tenuata*) were picked from the >150 μm fraction. *B. tenuata* was used only when *U. akitaensis* was absent (Table S1 in the auxiliary material), which was the case exclusively in laminated intervals.[1]

[14] Benthic foraminifera in PC-23A are well preserved based on observation under the microscope. An exception occurs between 1380 and 1400 cm below seafloor (cmbsf), where they show signs of dissolution, and such specimens have not been employed in this study. Benthic foraminiferal samples were analyzed at the Woods Hole Oceanographic Institution using an isotope ratio mass spectrometer (IRMS) Finnigan MAT 253. Oxygen and carbon isotope data were calibrated with an NBS-19 standard and expressed relative to Pee Dee belemnite (PDB) using conventional δ notation in ‰. The instrumental precision was <0.09‰ for $\delta^{18}O_{bf}$ and <0.07‰ for $\delta^{13}C_{bf}$.

[15] The shallow infaunal *U. akitaensis* has been previously shown to calcify its test close to the calcite oxygen isotope equilibrium [*Shackleton*, 1974]. Accordingly, $\delta^{18}O_{bf}$ reflects the $\delta^{18}O$ value and temperature of the local bottom water. The $\delta^{18}O$ of the local bottom water, in turn, reflects $\delta^{18}O$ of the average seawater, which is approximately represented by the benthic $\delta^{18}O$ stack [e.g., *Lisiecki and Raymo*, 2005], and the salinity deviation of the local bottom water from the average seawater. In our data, $\delta^{18}O_{bf}$ values of the shallow infaunal *B. tenuata* are consistent with $\delta^{18}O_{bf}$ values measured on *U. akitaensis* (Table S1), and are also used in this study.

[16] On the other hand, $\delta^{13}C$ of the shallow infaunal *Uvigerina* is offset from bottom water $\delta^{13}C$ by as much as −0.8‰ due to influence of pore water $\delta^{13}C$, which largely depends on the organic carbon rain rate at shallow infaunal depths [*McCorkle et al.*, 1990, 1997]. Since pore water $\delta^{13}C$ decreases through decomposition of organic matter settling from above during the course of lateral advection of the water [*Kroopnick*, 1985; *Matsumoto et al.*, 2002], $\delta^{13}C_{bf}$ variations may be interpreted in terms of changes in the organic carbon rain rate and/or changes in intermediate water ventilation. Precision of the $\delta^{13}C$ and $\delta^{18}O$ estimate for *Uvigerina* is ±∼0.16‰ (1σ) due to intraspecific variabilities in the isotopic disequilibrium of $\delta^{13}C$ and $\delta^{18}O$ [*Graham et al.*, 1981]. We use occurrences of laminations and/or the shallow infaunal *B. tenuata* as indicators of low oxygen on the sediment surface [e.g., *Kennett et al.*, 2000].

[17] While in most samples of PC-23A foraminifera are exclusively of clear white color, foraminiferal shells with unusual yellow color are included at specific horizons, which are typically characterized by more negative $\delta^{13}C_{bf}$ values as follows: −2.4‰ at 1601 cmbsf, −1.3 to −2.9‰ between 1235 and 1262 cmbsf, −2.0% at 1171 cmbsf, −1.5 to −1.7‰ between 998 and 1008 cmbsf, and −1.7‰ at 575 cmbsf (Table S1). Because such samples may have been influenced by authigenic carbonate overgrowth due to methane oxidation within the near surface sediments [*Cook et al.*, 2011; *Uchida et al.*, 2008], their $\delta^{13}C_{bf}$ values are not used in this study.

[1] Auxiliary materials are available in the HTML. doi:10.1029/2011PA002205.

Table 1. The ^{14}C and Calendar Ages of Planktonic Foraminifera in Core PC-23A[a]

ID	Plankt. Species	Depth [cm]	Libby Age [^{14}C ka]	Analytical Error [yr]	Cal. Age (-2σ) [ka BP]	Cal. Age ($+2\sigma$) [ka BP]	Cal. Age (Med) [ka BP]	Total Error (Lower Limit) [yr]	Total Error (Upper Limit) [yr]
1–13*	*N.p.*	27.9	10.47	130	10.69	11.40	11.11	915	899
1–25	*G.b.*	55.3	10.66	67	11.20	11.49	11.33	564	708
2–3*	*N.p.*	63.5	10.62	103	11.11	11.76	11.31	681	1030
2–21*	*N.p.*	104.3	11.03	71	11.75	12.37	12.04	732	885
3–17*	*G.b.*	205.6	11.93	66	12.84	13.26	13.08	671	731
3–34*	*N.p.*	244.5	12.47	67	13.42	13.78	13.59	605	736
3–34	*G.b.*	244.5	12.59	75	13.49	13.85	13.69	646	716
4–13*	*G.b.*	297.2	12.83	101	13.70	14.16	13.93	707	806
5–2*	*G.b. + N.p.*	373.0	13.25	69	14.17	15.09	14.62	885	1021
5–21*	*G.b.*	416.2	13.48	95	14.52	15.65	15.07	1019	1154
6–25*	*G.b. + N.p.*	524.4	16.35	135	18.60	19.04	18.82	726	843
7–9*	*G.b. + N.p.*	588.6	18.84	87	21.33	22.04	21.59	716	1010
7–39	*G.b. + N.p.*	656.7	21.47	173	24.29	25.17	24.74	998	1082
7–40*	*G.b. + N.p.*	659.0	21.40	97	24.38	25.03	24.69	775	919
11–9*	*G.b. + N.p.*	1007.6	33.32	198	36.60	37.76	37.04	2568	2678
12–16*	*N.p.*	1123.4	34.38	183	37.66	38.97	38.52	2553	2663
13–19	*G.b.*	1262.0	35.52	216	39.03	40.58	39.84	2586	2696
13–20	*G.b.*	1264.2	36.14	216	39.97	41.32	40.69	2586	2696
13–21*	*G.b.*	1266.5	37.56	284	41.31	42.27	41.80	2654	2764
14–32	*G.b.*	1397.9	30.81	172	34.52	35.14	34.77	2542	2652
16–01*	*G.b + N.p.*	1533.1	44.56	497	45.76	48.34	46.81	2867	2977

[a]The ^{14}C analyses were performed at the AMS facility of the National Institute for Environmental Studies (NIES-TERRA). Calendar age conversions were performed using Intcal/Marine09 [*Reimer et al.*, 2009] (ka BP = 1000 years before present). Planktonic species: G.b. = *G. bulloides*; N.p. = *N. pachyderma*. For ^{14}C ages younger than 24 ka, total error includes the analytical error, the 2σ calibration error and the uncertainty in reservoir age. For ^{14}C ages older than 24 ka, total error includes the analytical error, the uncertainty in reservoir age and an assumed uncertainty in radiocarbon calibration of $\pm$2000 years as outlined in the text. Asterisk indicates radiocarbon dates used in this study.

5.5. Radiocarbon Measurements

[18] To estimate ages of sediments in PC-23A, ^{14}C of planktonic foraminifera *Neogloboquadrina pachyderma* and *Globigerina bulloides* were measured at the NIES-TERRA Accelerator Mass Spectroscopy facility of the National Institute for Environmental Studies in Tsukuba, Japan. Samples were washed with tap water over a 63 μm screen, rinsed in distilled water and then dried at 50°C. Planktonic foraminifera were handpicked from samples, and then cleaned by soaking in 30% hydrogen peroxide solution to remove adhering contaminants. If abundance was high enough, single species (left-coiling *N. pachyderma* or *G. bulloides*) were used for dating. Otherwise, mixed species of *N. pachyderma* and *G. bulloides* were employed. Cleaning and graphitization of foraminifera at NIES-TERRA were carried out according to procedures after *Uchida et al.* [2004, 2005]. Resulting ^{14}C ages, analytical precisions, calendar ages and their 2σ uncertainties are listed in Table 1.

6. Lithology of PC-23A

[19] Sediments in core PC-23A were classified according to the ODP classification scheme [e.g., *Ingle et al.*, 1990]. According to smear slide observation, the sediments are composed of siliceous and calcareous biogenic remains such as diatoms, radiolarians, nanofossils and foraminifera, and siliciclastic grains including quartz, feldspar, clay minerals and lithics with occasional contribution of volcanic glass shards. The degree of lamina preservation and/or bioturbation is commonly related to bottom water oxygenation levels, and classified as laminated, bioturbated (i.e., distinct burrows are identified) or strongly bioturbated (i.e., homogeneous in appearance) [e.g., *Watanabe et al.*, 2007].

[20] A lithological column of PC-23A is shown in Figure 2. The core is dominantly composed of dark olive gray, gray or olive black silty clay, which is calcareous and/or siliceous to various extent and generally associated with pyrite-filled small burrows oblique to bedding (Figure 2a) or with patches of very fine sand sub-parallel to bedding (Figure 2b). Burrows generally have penetration depths of $\sim$1 cm and rarely exceed 4 cm after compaction. Laminated diatomaceous silty clay occurs at five intervals in the upper part and at one interval in the lowest part of PC-23A (Figure 2c). The lamination is characterized by alternation of olive black diatomaceous laminae with fromboidal pyrite and gray silty clay laminae with rare diatoms. Laminae, usually 1–2 mm thick, have distinct and continuous boundaries suggesting absence of bioturbation. Two to twenty-six cm thick layers of very fine sand are occasionally intercalated (Figure 2d). A sharp contact is observed in X-ray radiographs at $\sim$25 $\pm$ 1 cmbsf. One vitric ash layer was identified between 147 and 154 cmbsf.

7. Age Model for PC-23A

[21] Twenty-one samples were selected for ^{14}C measurements from horizons with relatively high abundance of planktonic foraminifera. Raw ^{14}C data were calculated to conventional ^{14}C ages using the Libby half-life [*Stuiver and Polach*, 1977], and converted to calendar ages using the Intcal/Marine09 calibration curve [*Reimer et al.*, 2009] and the Calib 6.0 software [*Stuiver and Reimer*, 1993]. For radiocarbon ages older than $\sim$30 thousand years (ka), radiocarbon age calibration becomes less well constrained due to larger uncertainties in the atmospheric $\Delta^{14}C$ inventory and surface water reservoir ages, and limited availability of calibration data sets [*Reimer et al.*, 2009]. Taking into

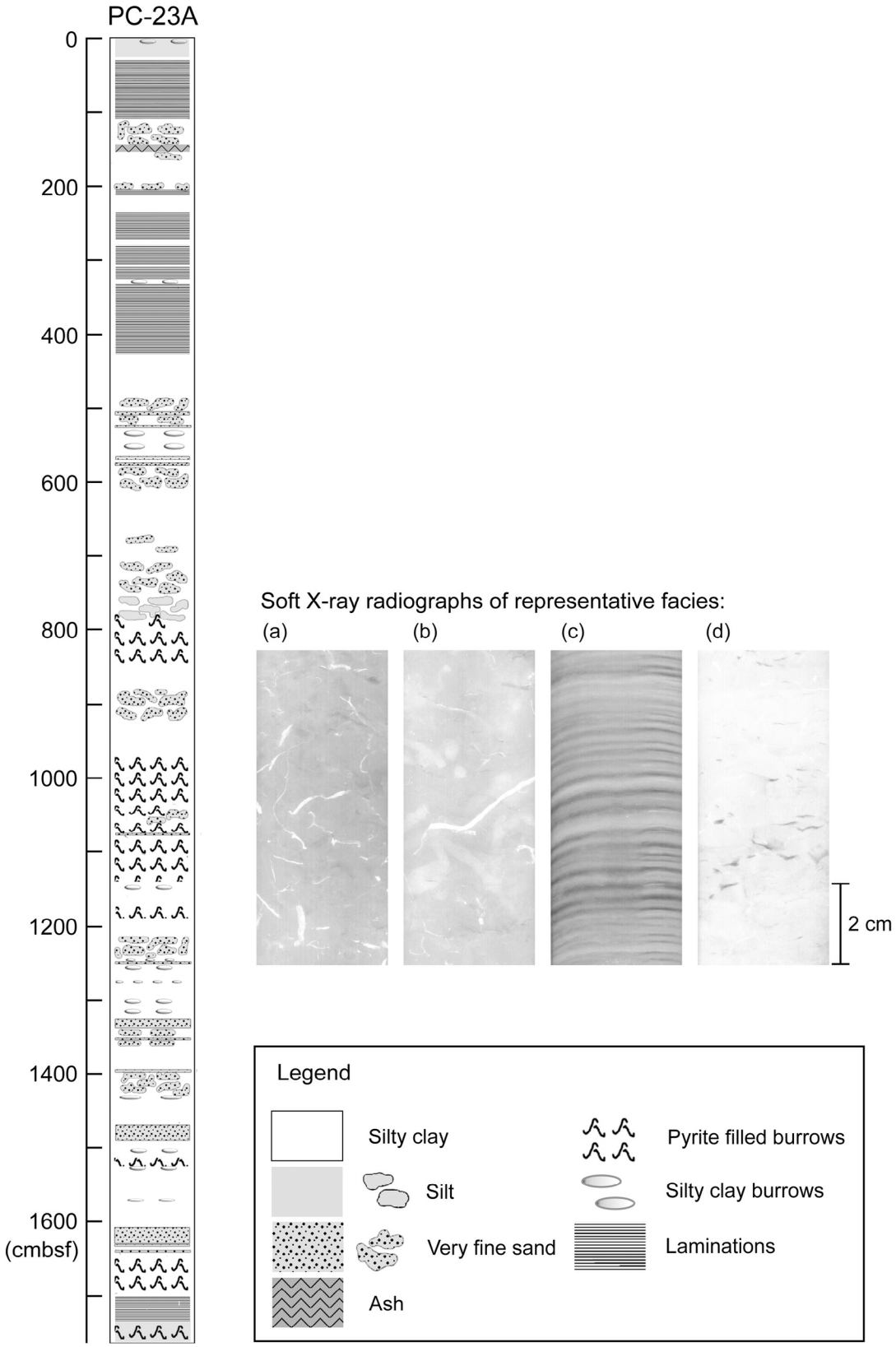

Figure 2. Columnar section of PC-23A. Also shown are soft X-ray photographs of major sedimentary facies: (a) bioturbated silty clay with burrows in the form of filaments (1176–1184 cmbsf), (b) bioturbated silty clay with burrows in the form of very fine sand patches (1242–1249 cmbsf), (c) laminated diatomaceous silty clay (355–363 cmbsf), and (d) bioturbated or strongly bioturbated very fine sand (1468–1476 cmbsf).

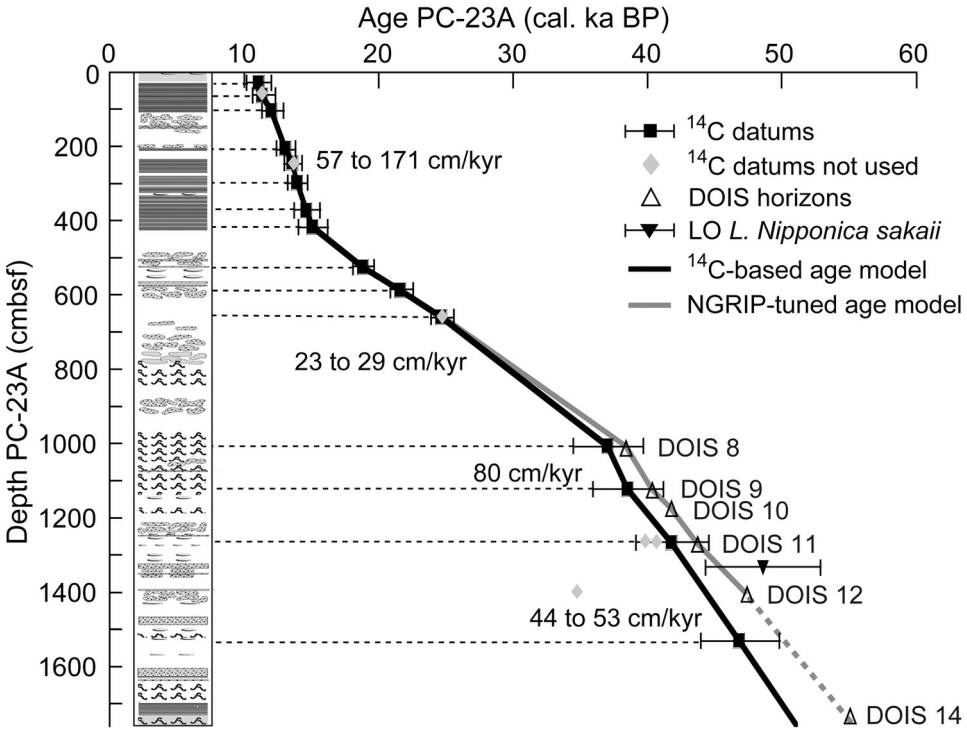

Figure 3. A diagram showing the relation between depth and calendar age for PC-23A. The black line illustrates the ^{14}C-based age model and the gray line illustrates the NGRIP-tuned age model for ages older than 24 cal. ka before present (BP). Black rectangles with error bars are ^{14}C datums used in this study, and gray diamonds ^{14}C datums not used. The black reversed triangle with error bar is LO *L. nipponica sakaii.* The open triangles indicate bases of prominent %$CaCO_3$ peaks when correlated to bases of NGRIP DOIS 8 to 12 and 14 (cf. correlation lines in Figure 4). The error bars of ^{14}C datums indicate the lower and upper limit of total error (cf. Table 1). Sedimentation rates and the lithological column are also shown. The legend for the columnar section is the same as in Figure 2.

account considerable variability in the different ^{14}C calibration data sets (±∼1000 years) for ^{14}C ages older than ∼30 ka [*Reimer et al.*, 2009], the relatively large sparsity of calibration data points during the same period in Intcal/Marine09 [*Reimer et al.*, 2009], and unknown reservoir ages during MIS 3, a calibration error of ±2000 years for ^{14}C ages older than 30 ka is assumed in this study.

[22] Calendar ages were corrected assuming a 780 year reservoir age, which is the sum of the 400 year global surface water reservoir age [*Stuiver and Braziunas*, 1993] and a regional reservoir age (ΔR) of 380 years, assumed for the modern Bering Sea and subarctic North Pacific [e.g., *Robinson and Thompson*, 1981; *Dumond and Griffin*, 2002; *Kuzmin et al.*, 2002]. Between 23 and 14 ka before present (hereafter "ka" denotes "ka before present"), surface water reservoir ages of 300 to 1150 years have been determined for the terminal region of the thermohaline circulation (subarctic North Pacific) [*Sarnthein et al.*, 2007]. This uncertainty in reservoir ages (±∼400 years) is included in the total error assessment of radiocarbon dates (Table 1 and Figure 3).

[23] Results of ^{14}C measurements, in part previously published in *Itaki et al.* [2009] for calendar ages younger than 38 ka, are listed in updated form in Table 1. An age-depth diagram is presented in Figure 3. Calendar ages are shown as minimum, maximum and median values, which represent the range of analytical uncertainties. Total error of calendar ages older than 24 ka are the sum of uncertainties in the reservoir age, the calendar age calibration and the ^{14}C analytical precision. The total error range is illustrated also in Figure 3.

[24] At the depth of 244.5 cmbsf (sample 3–34) both *N. pachyderma* and *G. bulloides* have been measured. The two ages disagree by 135 years, which is within the aggregate error of measurement precision, but also could be due to the error associated with bioturbation as this sample is from a non-laminated interval. In this study, we employed the age determined for *N. pachyderma.*

[25] Calibrated ages increase with depth with three exceptions. Sample 2–3 is younger than sample 1–25 by ∼20 years in calendar age, which is within the analytical error considering that the two samples are stratigraphically only 8.17 cm apart. As for sample 3–34, we chose the ^{14}C age measured for *N. pachyderma* (sample 2–3) for our age model. Sample 7–40 is younger than sample 7–39 by ∼80 years in calendar age, which also is within the analytical error of these two neighboring samples that are 2.3 cm apart. We used the age of sample 7–40 for the age model, as it has a smaller analytical uncertainty than sample 7–39. The third exception is sample 14–32 at 1397.9 cmbsf with a calendar age of 36.17 ka, which is younger than the five overlying radiocarbon dates. Because PC-23A shows no sediment disturbances based on visual core description and

X-ray radiographs, we find it unlikely that sample 14–32 was contaminated by younger foraminifera from depths of ~950 cm or above, where calendar ages of less than ~37 ka are expected, especially in view of reasonable calendar ages between 950 and 1300 cm depth. Further research is thus required to determine the reason for the obviously too young age. In this study, sample 14–32 is not employed for the age model.

[26] Radiocarbon values of the neighboring samples 13–19 (1262.0 cmbsf), 13–20 (1264.2 cmbsf) and 13–21 (1266.5 cmbsf) agree within ~2 kyr, which are within the range of total error. From these three radiocarbon dates we used the calendar age of sample 13–21 (41.95 ± ~2.7 ka), as it contained the largest amount of *G. bulloides* and corresponds to a $\%CaCO_3$ maximum (peak), where dating error due to bioturbation is minimized.

[27] In order to independently crosscheck our radiocarbon-based age model, we also show in Figure 3 the last occurrence (LO) of the radiolarian species *Lychnocanoma nipponica sakaii* in PC-23A [*Itaki et al.*, 2009], which is widely recognized in the northern Pacific and in the Okhotsk Sea at ~50 ka [*Morley and Nigrini*, 1995; *Okazaki et al.*, 2003]. This event was dated as 48.6 ± 1.8 ka based on correlation of paleointensity records from several Bering Sea cores, in which LO of *L. nipponica sakaii* were identified, with the global paleointensity stack GLOPIS-75 of *Laj et al.* [2004] [*Okada et al.*, 2005]. Calendar age uncertainty in GLOPIS-75 for ages older than 40 ka is at least ±2 kyr [*Laj et al.*, 2004; *McMillan and Constable*, 2006; *Singer et al.*, 2009]. LO of *L. nipponica sakaii* occurred at a depth between 1330 and 1340 cmbsf in PC-23A, which implies an additional error of 0.23 kyr due to depth uncertainty of ±5 cm, when linearly interpolating between radiocarbon age control points. Thus estimated LO of *L. nipponica sakaii* at 48.6 ± 4 ka is consistent within error limits with the radiocarbon-based age estimation (Figure 3).

[28] We applied linear interpolation between the age control points. As shown in Figure 3, the sedimentation rate is ~53 cm/kyr between core bottom (1758 cmbsf; ~51.1 ka) and 1267 cmbsf (~41.8 ka), ~44 cm/kyr between 1267 and 1124 cmbsf (~41.8 and ~38.5 ka), ~80 cm/kyr between 1124 and 1006 cmbsf (~38.5 and ~37.0 ka), slower at 23 to 29 cm/kyr in the interval between 1006 and 416 cmbsf (~37.0 and ~15.1 ka), and generally faster in the range of 57 to 171 cm/kyr between 416 and 28.1 cmbsf (~15.1 and ~11.1 ka). Based on a study of ^{210}Pb on a multicore (MC-25) taken from the same site as PC-23A, the core top age is estimated as younger than 200 years (N. Harada, unpublished data, 2007). Hence, we consider the sharp contact at ~25 ± 1 cmbsf as a non-depositional surface (hiatus) that spans the interval between ~11.1 and ~0.2 ka.

8. Results

8.1. The $\delta^{18}O$ Variation of Benthic Foraminifera

[29] The $\delta^{18}O_{bf}$ in PC-23A are presented in Figure 4f, jointly with their 2-point moving average, in order to filter decadal to centennial-scale noise and to emphasize millennial-scale variations. During MIS 3, the $\delta^{18}O_{bf}$ data range between 4.7 and 4.2‰ and are characterized by variations of 0.2 to 0.5‰ in amplitude with maxima observed at ~49, ~45, ~43, ~38, ~35 and ~30 ka. Between ~27 and ~18.7 ka (during MIS 2), $\delta^{18}O_{bf}$ are higher than during MIS 3, ranging from 4.6 to 4.9‰ with maxima at ~27, ~21 and ~18.7 ka. The rapid deglacial decrease in $\delta^{18}O_{bf}$ begins at ~18.7 ka, which agrees in timing with the initial melting of ice sheets and eustatic sea level rise [*Yokoyama et al.*, 2000; *Dyke et al.*, 2002]. Between ~18.7 ka and the earliest Holocene, $\delta^{18}O_{bf}$ steeply decreases from 4.9‰ toward a minimum of 3.5‰ at ~11 ka. The $\delta^{18}O_{bf}$ decrease is interrupted by two plateaus of rather constant $\delta^{18}O_{bf}$ values between ~18.0 and ~16.1 ka, and ~13.0 and ~12.1 ka, respectively, which are called "$\delta^{18}O_{bf}$ plateaus" in this study (Figure 5c).

8.2. The $\delta^{13}C$ Variation of Benthic Foraminifera

[30] The $\delta^{13}C_{bf}$ in PC-23A are presented in Figure 4e together with their 2-point moving average (averaging was not applied over intervals, where $\delta^{13}C_{bf}$ data is missing due to absence of *U. akitaensis* or occurrences of yellowish foraminifera). At orbital scales, $\delta^{13}C_{bf}$ slightly decreases from −1.1‰ at ~50 ka to −1.9‰ at ~47 ka, then increases to −0.7‰ at ~38 ka, and shows an average value of −1.0‰ between 38 and 30 ka. After 30 ka, $\delta^{13}C_{bf}$ decreases to −1.5 ‰ at ~22.5 ka and increases again to −0.5‰ at ~11 ka (Figure 4e). Superimposed on this orbital-scale trend, millennial-scale variations of 0.2 to 0.6‰ in amplitude are evident. During deglaciation $\delta^{13}C_{bf}$ show two maxima between ~17.3 and ~15.9 ka, and ~12.9 and ~12.1 ka, which are interrupted by low $\delta^{13}C_{bf}$ values between ~15.3 and ~13.0 ka that approximately correspond to a laminated interval (Figures 4 and 5d). It is worth to note that laminations start ~500 years after the onset of the strong decrease in $\delta^{13}C_{bf}$ at ~15.6 ka. The low-oxygen benthic species *B. tenuata* is common all through the interval from ~15.6 to ~13.0 ka, suggesting that oxygen levels of intermediate water remained low during this period.

Figure 4. Temporal variations of (a) $\delta^{18}O_{bf}$ in PC-23A (in gray; based on the NGRIP-tuned age model (see text)) and XP98-PC1 (in black and dashed; *Sakamoto et al.* [2005]), (b) $\delta^{18}O$ in the NGRIP ice core [*North Greenland Ice Core Project Members*, 2004], (c) $\%CaCO_3$ in PC-23A (3-point average), (d) semiquantitative estimate of absolute abundances of planktonic foraminifera (p.f.) in PC-23A, in ranks from 0 (absent or rare) to 5 (abundant), (e) $\delta^{13}C_{bf}$ in PC-23A (gray curve: raw data; black curve: 2-point average), and (f) $\delta^{18}O_{bf}$ in PC-23A (gray curve: raw data; black curve 2-point average), and their association with Heinrich events, DOS and DOIS recorded in $\delta^{18}O$ of the NGRIP ice core. (g) The lithological column of PC-23A is also shown. The legend of the columnar section is the same as in Figure 2. Crosses below Figures 4a and 4f are radiocarbon datums (normal: PC-23A; bold: XP98-PC1). Below Figure 4a, reversed open triangles are MIS datums, the reversed filled triangle is a tephra horizon in XP98-PC1, and open triangles indicate bases of NGRIP DOIS 8 to 12 and 14 that are used as age controls for the NGRIP-tuned age model of PC-23A and are correlated to $\%CaCO_3$ of PC-23A by dashed correlation lines. Shaded zones are defined by $\delta^{13}C_{bf}$ maxima in PC-23A, which can be correlated to NGRIP stadials.

8.3. Variations in %$CaCO_3$

[31] Microscopic observation revealed that the variations in %$CaCO_3$ dominantly reflect variations in the absolute abundance of planktonic foraminifera (Figures 4c and 4d) and only to a minor degree benthic foraminifera abundances or the occasional presence of authigenic carbonate. %$CaCO_3$ is highly variable prior to 36 ka with prominent peaks repeated every few thousand years. It is relatively low but

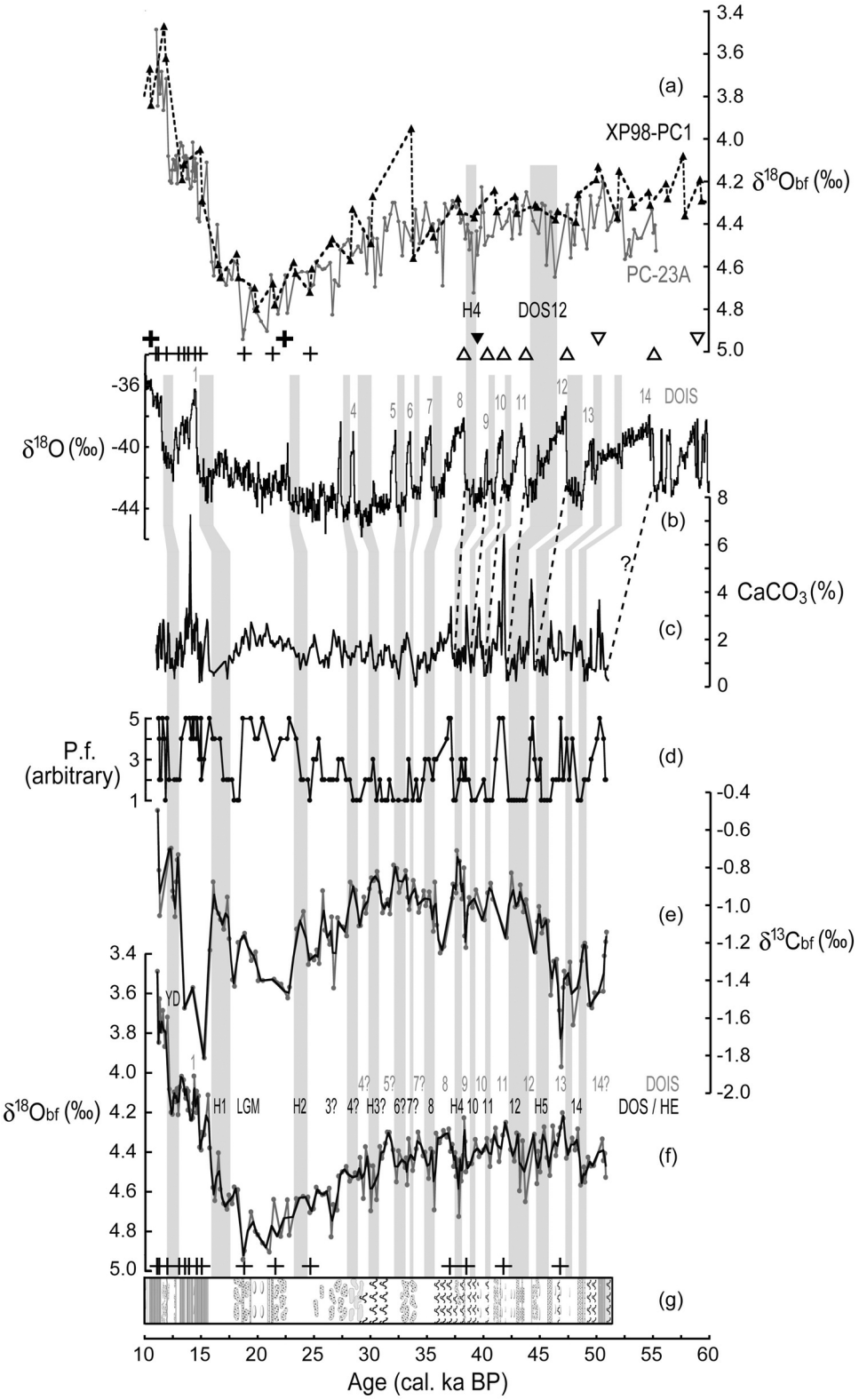

Figure 4

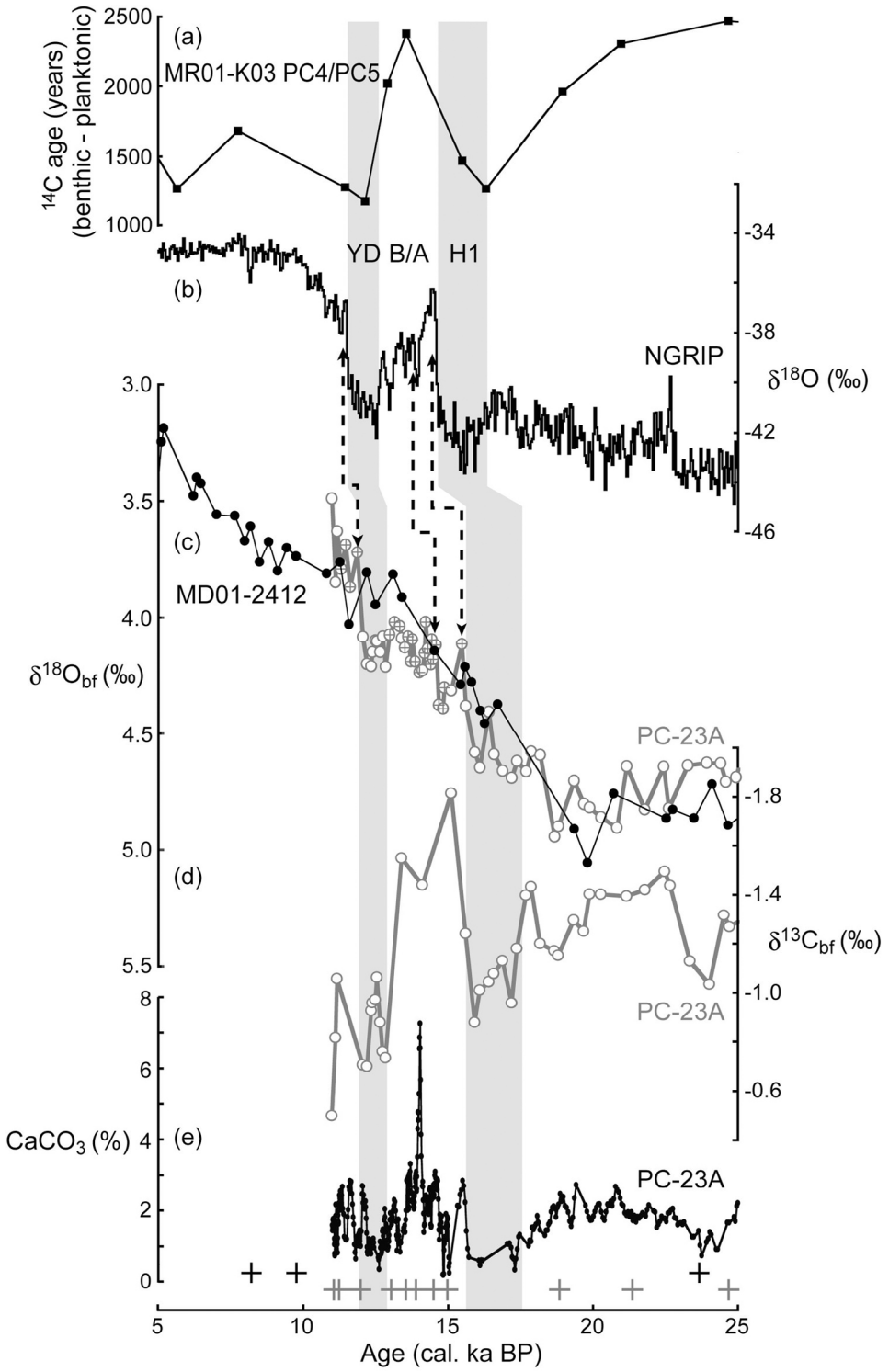

Figure 5. Temporal variations of (a) benthic minus planktonic radiocarbon ages in PC4/PC5 [*Ahagon et al.*, 2003], (b) $\delta^{18}O$ in the NGRIP ice core [*North Greenland Ice Core Project Members*, 2004], (c) $\delta^{18}O_{bf}$ in MD01–2412 [*Sakamoto et al.*, 2006] with additional $\delta^{18}O_{bf}$ from M. Ikehara (unpublished data, 2009) (in black) and $\delta^{18}O_{bf}$ in PC-23A (in gray), (d) $\delta^{13}C_{bf}$ in PC-23A (in gray), and (e) $\%CaCO_3$ in PC-23A for the time period between 5 and 25 ka. $\delta^{18}O_{bf}$ and $\delta^{13}C_{bf}$ are based on *U. akitaensis*, except for $\delta^{18}O_{bf}$ data points designed as gray open circles with crosses that are based on *B. tenuata.* Shaded zones mark $\delta^{18}O_{bf}$ plateaus and $\delta^{13}C_{bf}$ maxima in PC-23A and their association with Heinrich event 1 (H1) and the Younger Dryas (YD). Dashed lines with arrows show the temporal offset between $\delta^{18}O_{bf}$ in PC-23A and $\delta^{18}O$ in NGRIP. Crosses are radiocarbon datums (gray: PC-23A; black: MD01–2412).

still variable from 36 to 24 ka, whereas it is rather stable at moderately high values from 24 to 18 ka (Figure 4c). During deglaciation $\%CaCO_3$ is low in the bioturbated intervals ($\sim$17.3 to $\sim$16.0 ka and $\sim$13.0 to $\sim$12.1 ka) and rather high in the dominantly laminated intervals between $\sim$15.6 and $\sim$13.0 ka (corresponding to the B/A period) as well as between $\sim$12.1 and $\sim$11.1 ka (earliest Holocene). A marked $\%CaCO_3$ peak occurs at $\sim$14.0 ka (Figures 4c and 5e). The temporal variation of $\%CaCO_3$ is consistent with $\%CaCO_3$ of PC-23A independently measured by a coloumbmeter [*Kim et al.*, 2008; *Itaki et al.*, 2009].

8.4. Relationship Between $\%CaCO_3$, $\delta^{18}O_{bf}$ and $\delta^{13}C_{bf}$, and Their Association With Greenland Ice $\delta^{18}O$

[32] The $\%CaCO_3$, $\delta^{18}O_{bf}$ and $\delta^{13}C_{bf}$ profiles of PC-23A are compared to each other and to the NGRIP $\delta^{18}O$ record [*North Greenland Ice Core Project Members*, 2004], in order to examine possible associations between D-O cycles and paleoceanographic changes recorded in the sediments at site MR06-04-23. *Gorbarenko et al.* [2005] correlated intervals of increased $\%CaCO_3$ during the last glacial and deglacial period in the southern Bering Sea to DOIS, because these intervals were also associated with increased abundances of planktonic foraminifera (in particular thermophilic species) and warm water diatom species. Also in PC-23A, the prominent $\%CaCO_3$ peak during deglaciation coincides with the B/A warm period, which is associated with a laminated interval as was also noted by *Cook et al.* [2005]. Thus, if we assume that the intervals of high $\%CaCO_3$ are associated with warm periods during the last glacial period, as is observed during the well-dated deglaciation, $\%CaCO_3$ peaks between 51 and 37 ka in PC-23A can be correlated to a suite of DOIS evident in the NGRIP $\delta^{18}O$ record, possibly to DOIS 14, 12, 11, 10, 9, and 8 (Figures 4b and 4c) within the error of our age model (<3 kyr). Between 37 and 25 ka, correlation of $\%CaCO_3$ peaks and NGRIP interstadials is more uncertain. Although a correlation of $\%CaCO_3$ peaks to DOIS 6, 5 and 4 is possible, it should be noted that not all $\%CaCO_3$ peaks can be matched to DOIS (Figures 4b and 4c).

[33] During deglaciation, the stepwise decreases in $\delta^{18}O_{bf}$ seem to lead similar decreases in $\delta^{18}O$ of NGRIP by $\sim$0.5 to $\sim$1 kyr (Figures 5b and 5c). The $\delta^{18}O_{bf}$ plateaus are associated with distinct positive excursions of $\delta^{13}C_{bf}$ (Figure 5d), low $\%CaCO_3$ (Figure 5e) and bioturbated intervals, and probably correlate to H1 and YD with apparent time leads of $\sim$1 kyr and $\sim$0.5 kyr, respectively (Figure 5). On the other hand, the interval between $\sim$15.5 and $\sim$13 ka, which is characterized by three consecutive $\delta^{18}O_{bf}$ minima, very low $\delta^{13}C_{bf}$ values (-1.4 to -1.8‰ based on *U. akitaensis*), high $\%CaCO_3$, and dominance of lamination, probably correlates to the B/A period with an apparent time lead of $\sim$1 kyr. Finally, the low values of $\delta^{18}O_{bf}$ after 12 ka that are coeval with $\%CaCO_3$ peaks and low $\delta^{13}C_{bf}$, probably correlate to the earliest Holocene with an apparent time lead of $\sim$0.5 kyr (Figure 5).

[34] Similarly, during the last glacial period, positive excursions of $\delta^{18}O_{bf}$ tend to coincide with positive excursions of $\delta^{13}C_{bf}$ and low $\%CaCO_3$ in PC-23A (Figure 4). If we assume that the association of higher $\delta^{18}O_{bf}$, higher $\delta^{13}C_{bf}$ and lower $\%CaCO_3$ with cold periods, as observed during deglaciation, is maintained during the last glacial period, positive excursions of $\delta^{18}O_{bf}$ and $\delta^{13}C_{bf}$, and low $\%CaCO_3$ correlate – within the error of our age model and under the constraints of our proposed correlation between $\%CaCO_3$ peaks and NGRIP interstadials – to Heinrich events 5, 4 and 3 (hereafter H5, H4, H3) and several DOS, tentatively to DOS 14, 12, 10, 8 and 6 (Figure 4). It should be noted that the positive $\delta^{13}C_{bf}$ excursion at $\sim$45 ka (tentatively correlated to H5) corresponds in the earlier part to a minimum and in the later part to a maximum of $\delta^{18}O_{bf}$. Positive $\delta^{13}C_{bf}$ excursions at $\sim$40 and $\sim$28 ka are associated with weak temporal $\delta^{18}O_{bf}$ increases. The positive $\delta^{13}C_{bf}$ excursion at $\sim$35 ka, possibly associated with DOS 8, is less pronounced. Also, the positive $\delta^{18}O_{bf}$ excursion at $\sim$27 ka, which might correlate to an episode of DOS 3, is associated with a generally weak $\delta^{13}C_{bf}$ increase, although this increase is interrupted by a single negative $\delta^{13}C_{bf}$ excursion. An exception to the general trend is the positive $\delta^{13}C_{bf}$ excursion at $\sim$24 ka, possibly corresponding to H2, which is associated with rather low $\delta^{18}O_{bf}$ values. On the other hand, negative excursions of $\delta^{18}O_{bf}$ and $\delta^{13}C_{bf}$ at $\sim$51, $\sim$44, $\sim$42, $\sim$38.5, $\sim$37 and $\sim$31 ka, which also correspond to $\%CaCO_3$ peaks, can be correlated to several DOIS, tentatively to DOIS 14, 12, 11, 9, 8 and 5 (Figure 4), although the decreases in $\delta^{18}O_{bf}$ are not as abrupt as the increases in $\%CaCO_3$.

[35] In summary, high $\delta^{18}O_{bf}$ and $\delta^{13}C_{bf}$ events probably correlate with H1 and YD during deglaciation and, under the above outlined assumptions, to Heinrich events and several DOS during MIS 3.

9. Discussion

9.1. Cold and/or Saline Intermediate Waters During the LGM in the Northeastern Aleutian Basin

[36] At site MR06-04-23 at $\sim$1000 m water depth, the water temperature is at present 2.8°C, salinity 34.37‰ (MR06–04 hydrological data), and $\delta^{18}O$ of seawater -0.7‰ PDB (A. Ijiri, personal communication, 2009). Using the relationship between water temperature and $\delta^{18}O_{bf}$ of *Shackleton* [1974] for *Uvigerina* species, the expected modern $\delta^{18}O_{bf}$ is $\sim$2.8‰, implying a $\delta^{18}O_{bf}$ difference of -1.8 to -2.1‰ between the LGM and modern settings. Accepting a change in $\delta^{18}O_{bf}$ of -1.0 ± 0.1‰ [*Schrag et al.*, 2002] due to ice volume changes between the LGM and present, the remaining -0.7 to -1.1‰ of the LGM and modern $\delta^{18}O_{bf}$ difference would be due to temperature and/or local salinity changes. Consequently, under the assumption that local salinity anomalies did not change between the LGM and early Holocene, LGM intermediate water temperature was between -0.2 and -2.0°C using a 0.23‰ increase in $\delta^{18}O_{bf}$ per 1°C decrease in temperature [*Epstein et al.*, 1953]. Alternatively, under the assumption of constant temperature, LGM salinity levels in the Bering Sea would have ranged between 36.1 and 37.1‰, if we use the equation

$$\delta^{18}O_{seawater} = 0.4 \times \text{salinity} - 14.4 \quad (3)$$

determined by isotopic analyses of seawater from 1000 to 10 m depth in proximity of site MR06-04-23 (Ijiri, personal communication, 2009). Although salinity of the deep LGM ocean could have reached 36.1 to 37.1‰ [*Adkins et al.*,

2002], these extreme values were probably not reached at 1000 m depth in the Bering Sea, because an intermediate water mass of relatively low salinity extended to site MR06-04-23 during the LGM according to oxygen and hydrogen isotope analyses of pore water in PC-23A and two other neighboring cores from 853 and 1157 m water depth [*Ijiri et al.*, 2009]. This implies colder than present intermediate water at site MR06-04-23, which is consistent with evidence from radiolarian assemblages that suggest the presence of an extended low-temperature intermediate water mass in the Bering Sea during the LGM [*Tanaka and Takahashi*, 2005].

9.2. Possible Causes of Millennial-Scale $\delta^{18}O_{bf}$ and $\delta^{13}C_{bf}$ Variations at Site MR06-04-23

[37] The millennial-scale $\delta^{18}O_{bf}$ maxima during the last glacial period and the $\delta^{18}O_{bf}$ plateaus during the deglacial period in PC-23A, which we tentatively correlated to Heinrich events H5, H4, H3 and H1, as well as YD and several DOS (Figure 4), are considered to reflect periodic emergence of colder and/or more saline intermediate waters on the upper part of the continental slope. These intervals are also associated with lower $\%CaCO_3$, lower biogenic silica contents [*Itaki et al.*, 2009] and higher $\delta^{13}C_{bf}$ values. Combined, our results could be interpreted in terms of increased ventilation at intermediate water depths and low surface productivity during severe cold periods. Primary production would have been limited during Heinrich events and DOS due to lower nutrient levels in the surface water and a prolonged ice-covered period over the slope [*Sancetta and Robinson*, 1983] that limits availability of light and accordingly the length of the blooming season. In addition, new production of nutrient-poor intermediate water in the Bering Sea tends to dilute the nutrient-rich waters derived from the deep North Pacific that upwell at the terminus of the thermohaline circulation, decreasing nutrient availability and productivity in Bering Sea surface waters.

[38] Decreases in $\delta^{13}C_{bf}$, on the other hand, can be attributed to higher organic carbon accumulation due to increased surface productivity, and/or decreased ventilation and consequent aging of the water mass. Coeval maxima in $\%CaCO_3$ and minima in $\delta^{13}C_{bf}$ in PC-23A at intervals, which we suggest to coincide with DOIS (Figure 4), are consistent with a scenario of enhanced surface productivity associated with poorer oxygenation within the surface sediment. An increase in oxygen demand within the sediments is also suggested by the occasional appearance of *B. tenuata* in those intervals. The $\%CaCO_3$ peaks and negative $\delta^{13}C_{bf}$ excursions in PC-23A also commonly coincide with lower $\delta^{18}O_{bf}$, which suggests a relationship between surface productivity and intermediate water temperature and/or salinity. Due to efficient delivery of nutrients through melting ice and upwelling from the deep Aleutian Basin, the Bering Sea is today characterized by high surface productivity, in particular along the Bering Sea Green Belt [*Springer et al.*, 1996]. A similar scenario could be drawn for warm episodes of the last glacial period, when a reduction or cessation of intermediate water ventilation, accompanied by warming and/or a salinity decrease of the intermediate water (lower $\delta^{18}O_{bf}$), could have facilitated upwelling of nutrient-rich North Pacific deep waters and, in conjunction with nutrients derived from melting ice, promoted higher surface productivity as suggested by increased $\%CaCO_3$ and lower $\delta^{13}C_{bf}$.

9.3. Possible Source of NPIW During the Last Glacial and Deglacial Period

[39] It is believed that the northwestern Pacific Ocean shallower than ~2000 m water depth was well ventilated during the last glacial period [*Keigwin*, 1998]. The source of its ventilation, however, is still under debate [e.g., *Matsumoto et al.*, 2002]. *Ohkushi et al.* [2003] interpreted an opposite glacial-interglacial abundance pattern of *Cyclado-phora davisiana*, which dwells in well-oxygenated water, between the Okhotsk Sea (interglacial) and the Bering Sea (glacial) as a source switch of NPIW between the two seas. Decreased ventilation at intermediate depths in the Okhotsk Sea during the last glacial period has also been proposed based on radiolarian abundances [*Okazaki et al.*, 2008].

[40] Today, seawater $\delta^{18}O$ between 750 and 1250 m depth in the Okhotsk Sea and northeastern Bering Sea is $-0.18 \pm 0.04‰$ (n = 73) and $-0.35 \pm 0.24‰$ (n = 5), respectively, based on the world ocean $\delta^{18}O$ database (G. A. Schmidt et al., Global Seawater Oxygen-18 Database v1.21, 1999, available at http://data.giss.nasa.gov/o18data/) and $\delta^{18}O$ measured at site MR06-04-23 (Ijiri, personal communication, 2009). These data suggest an average negative $\delta^{18}O_{bf}$ gradient between the Okhotsk Sea, where NPIW primarily forms, and the northeastern Bering Sea ($\Delta\delta^{18}O_{bf} = \delta^{18}O_{bf\ Bering} - \delta^{18}O_{bf\ Okhotsk}$). Such observation is consistent with our idea that the opposite situation, when NPIW formation in the Bering Sea surmounts that of the Okhotsk Sea, would be characterized by a positive $\Delta\delta^{18}O_{bf}$.

[41] We accordingly compared our $\delta^{18}O_{bf}$ record of the northeastern Bering Sea slope with that of the central Okhotsk Sea core XP98-PC1 [*Sakamoto et al.*, 2005] (Figure 4a), which is located at 51°00.9′N, 152°00.5′E (Figure 1), in order to explore the possibility of NPIW formation in the glacial Bering Sea. The water depth of XP98-PC1 (1107 m) is comparable with that of PC-23A. Site XP98–1 is located proximate to the modern source region of NPIW [e.g., *Shcherbina et al.*, 2003]. Age control points of XP98-PC1, which are based on oxygen isotope stratigraphy and tephrachronology in MIS 3 and radiocarbon dating at the LGM and deglaciation [*Sakamoto et al.*, 2005], are indicated in Figure 4a. Based on the proposed correlation between $\%CaCO_3$ peaks in PC-23A and DOIS in NGRIP for the interval older than 24 ka (Figures 3, 4b, and 4c), we construct a NGRIP-tuned age model for PC-23A, in an effort to minimize dating errors when comparing PC-23A and XP98-PC1. $\delta^{18}O_{bf}$ measurements on XP98-PC1 were carried out on *Uvigerina proboscidea* for the time period prior to 15.3 ka and *U. akitaensis* after 15.3 ka at Hokkaido University using an IRMS Finnigan MAT 251. Results were calibrated through a NBS-20 standard and expressed relative to PDB with an instrumental precision of <0.03‰ [*Sakamoto et al.*, 2005]. Both species gave identical $\delta^{18}O_{bf}$ values within error and are therefore suitable for a direct comparison to the $\delta^{18}O_{bf}$ record of PC-23A.

[42] In orbital scale, the two $\delta^{18}O_{bf}$ records are similar in shape and values, although PC-23A shows higher amplitude variations in $\delta^{18}O_{bf}$ during MIS 3 (Figure 4a). In both cores, $\delta^{18}O_{bf}$ increase during MIS 2 (LGM) and rapidly decrease simultaneously during deglaciation. Aggregate uncertainties in age estimation between XP98-PC1 and the NGRIP-tuned PC-23A record prior to ~25 ka allow us to discuss with

confidence only gross features such as the $\delta^{18}O_{bf}$ increases to ~4.7‰ at ~46 and ~39 ka, which we interpret to correspond to DOS 12 and H4, respectively. Even if considering the age uncertainties in the two age models and possible inter-machine and/or interlaboratory biases in $\delta^{18}O_{bf}$ analyses, which could be at the order of 0.1 to 0.2‰ [*Zahn and Mix*, 1991; *Ostermann and Curry*, 2000], $\delta^{18}O_{bf}$ of XP98-PC1 do not show such strong decreases as they are observed in PC-23A at ~46 and ~39 ka (Figure 4a). According to these data, therefore, a positive $\Delta\delta^{18}O_{bf}$ seems to have been established between the Bering and Okhotsk Seas at least during these two periods.

[43] We conclude from above considerations that intermediate water was colder and/or more saline in the Bering Sea than in the Okhotsk Sea during DOS 12 and H4 according to our correlation, and possibly during other cold periods such as DOS 14 and H3. At intervals, which we correlated to DOIS, on the other hand, the two cores show rather similar $\delta^{18}O_{bf}$ values suggesting absence of strong temperature and/or salinity gradients at intermediate water depth between the Bering and Okhotsk Seas. It should be noted that due to the limits of our age model, we cannot exclude the possibility that a positive $\Delta\delta^{18}O_{bf}$ could have started during the late part of DOIS 12 (Figures 4a and 4b). While further study is needed to better constrain the timing of $\Delta\delta^{18}O_{bf}$ increases, we suggest at this stage, in line with our discussion in chapter 8.4 on increases of $\delta^{18}O_{bf}$ during cold periods in the Bering Sea, that the establishment of positive $\Delta\delta^{18}O_{bf}$ would have been largely a feature of cold periods.

[44] Based on paired benthic-planktonic foraminiferal ^{14}C age differences in the piston cores MR01-K03 PC4 and PC5 at 1366 m water depth off Shimokita peninsula in northeastern Japan, *Ahagon et al.* [2003] proposed enhanced ventilation between ~17 and ~15 ka, and ~12.5 and ~11.4 ka corresponding to H1 and YD, respectively, and relatively sluggish ventilation between ~15 and ~12.5 ka corresponding to the B/A period (Figure 5a). In order to obtain information on the source region(s) and direction of lateral advection of intermediate water during these abrupt deglacial ventilation changes off Shimokita, we compared $\delta^{18}O_{bf}$ from PC-23A with those from piston core MD01–2412, which are also based on *U. akitaensis* [*Sakamoto et al.*, 2006; M. Ikehara, unpublished data, 2009] (Figure 5c). $\delta^{18}O_{bf}$ of MD01–2412 were analyzed at Kochi University using an IRMS IsoPrime GV Instruments. Results were calibrated through a NBS-19 standard and expressed relative to the Vienna PDB with an instrumental precision of <0.03‰ [*Sakamoto et al.*, 2006]. MD01–2412 is located geographically near PC4/PC5 at 44°31.65′N, 145°00.25′E in the southwestern Okhotsk Sea at a water depth of 1225 m (Figure 1).

[45] The $\delta^{18}O_{bf}$ plateaus of PC-23A that correspond to H1 and YD are ~0.3‰ higher than respective $\delta^{18}O_{bf}$ values in MD01–2412 (Figure 5c), although it should be noted that $\Delta\delta^{18}O_{bf}$ may range between 0.1 and 0.5‰ during these periods due to possible inter-machine and/or interlaboratory biases in $\delta^{18}O_{bf}$ analyses [*Zahn and Mix*, 1991; *Ostermann and Curry*, 2000]. The observed positive $\Delta\delta^{18}O_{bf}$ may suggest that the source region of better ventilated intermediate waters during H1 and YD [*Duplessy et al.*, 1989; *Ahagon et al.*, 2003] was proximate to the northern Bering Sea rather than the Okhotsk Sea, supporting the view that lateral advection of intermediate water occurred from the Bering Sea to the southwestern Okhotsk Sea.

[46] Between ~15.3 and ~13.0 ka, a period approximately corresponding to the B/A period and mostly laminated in PC-23A, $\delta^{18}O_{bf}$ values in PC-23A and MD01–2412 are similar (Figure 5c), suggesting that the two regions were bathed by the same water mass, which could be linked to reduction or cessation of intermediate water formation in the Bering Sea. During the same period, $\delta^{13}C_{bf}$ (based on *U. akitaensis*) are very low in PC-23A (Figure 5d), suggesting increased organic carbon flux and/or decreased ventilation. A reduction in intermediate water ventilation in the Bering Sea during the B/A period could be causally linked to the synchronous reduction in ventilation off Shimokita peninsula [*Duplessy et al.*, 1989; *Ahagon et al.*, 2003]. Ventilation was also reduced off Shimokita peninsula during the late LGM (Figure 5a), which is associated with absence of a significant lateral $\delta^{18}O_{bf}$ gradient between PC-23A and MD01–2412 (Figure 5c), suggesting a rather stagnant condition of the intermediate water.

[47] Hence, increases in intermediate water ventilation off Shimokita peninsula during H1 and YD [*Duplessy et al.*, 1989; *Ahagon et al.*, 2003] are consistent with colder and/or more saline intermediate water (NPIW) production in the Bering Sea, and its lateral advection to the region off northeastern Japan. Our results therefore support the Bering Sea as a source of NPIW during severe cold periods such as DOS 12, H4, H1 and YD and reduction or absence of NPIW production in the Bering and Okhotsk Seas during interstadial periods.

9.4. Northern Hemispheric Cooling and Associated Atmospheric Reorganization During Stadial Periods as Triggers of NPIW Formation in the Bering Sea

[48] The benthic isotopic records in PC-23A and their comparison with those in the Okhotsk Sea as well as with ventilation changes off northeastern Japan demonstrate the potential importance of the Bering Sea as a source of the ventilated intermediate water masses observed in the glacial North Pacific [*Keigwin*, 1998; *Duplessy et al.*, 1989; *Matsumoto et al.*, 2002]. Our results are also consistent with the hypothesis of *Ohkushi et al.* [2003], who advocated the occurrence of better ventilated intermediate water in the Bering Sea during the last glacial period based on radiolarian assemblages. Using a coupled ocean-atmosphere climate model, *Kim and Park* [2008] suggested significant increases in surface water densities in the Bering Sea during the last glacial period due to surface water cooling and salinity increases, which would primarily have resulted from a decrease in the precipitation/evaporation ratio over the northern North Pacific. The associated destabilization of the water column could have effectively contributed to NPIW formation in the northern marginal seas of the North Pacific [*Kim and Park*, 2008]. A positive salinity feedback arising from a compensatory northward transport of saline subtropical Pacific surface waters could have further enhanced NPIW formation in the Bering Sea. However, our results suggest that NPIW formation – at least in the Bering Sea – was not necessarily active all through the glacial period, but only during severe cold periods, such as Heinrich events and some DOS.

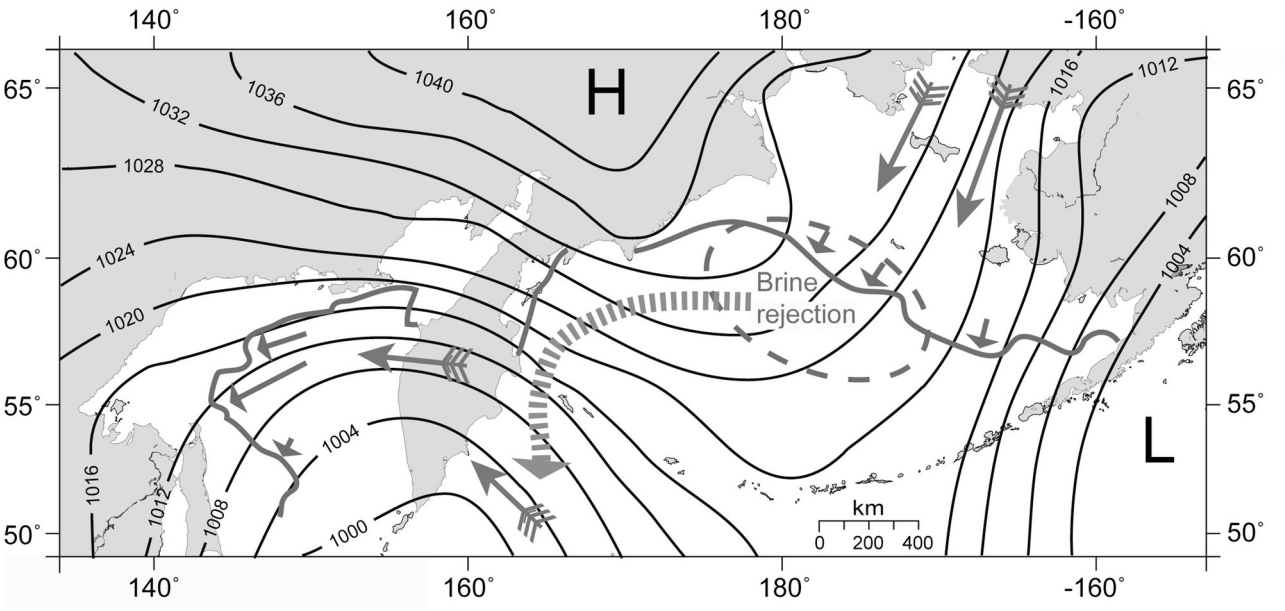

Figure 6. Map of the Bering and Okhotsk Sea region showing sea level pressure patterns (values in hPa) and sea ice extents of March 15th, 1976 (redrawn from *Cavalieri and Parkinson* [1987]). Siberian High and Aleutian Low are designated by H and L, respectively. Sea ice extents in the Bering and Okhotsk Seas are indicated by gray lines. Simple continuous arrows mark the extent of sea ice advance or retreat compared to March 6th, 1976 [*Cavalieri and Parkinson*, 1987]. Dominant winds are indicated by continuous arrows with tails. The area of possible intensified brine rejection and NPIW formation during severe cold stadials, and consequent NPIW outflow to the North Pacific are indicated by a dashed oval and a dashed thick arrow, respectively.

[49] An important mechanism that may modulate surface water densities and thereby constrain the timing and location of intermediate water formation is the rejection of brine during sea ice formation around persistent polynyas [e.g., *Talley*, 1991; *Shcherbina et al.*, 2003; *Haley et al.*, 2008]. Such ice-free zones are often created when dominant winds from the continent push sea ice away from the coast. The generated dense water sinks to depths until a new density equilibrium with the surrounding water masses is reached. Such process is believed to be a primary control on NPIW formation in the modern Okhotsk Sea [e.g., *Talley*, 1991, 1993; *Yasuda*, 1997].

[50] Today, cold northerly winds over the Okhotsk Sea are associated with the Aleutian Low over the Okhotsk Sea region and the Siberian High over central Siberia and northern China [e.g., *Cavalieri and Parkinson*, 1987]. The coldest winters in the Bering Sea, on the other hand, occur when the Aleutian Low is displaced to the east and anomalously high pressure dominates over northeastern Siberia favoring northerly winds over the Bering Sea [*Luchin et al.*, 2002; *Rodionov et al.*, 2007] (Figure 6). In accordance with these observations, *Cavalieri and Parkinson* [1987] reported episodic out of phase relationships in sea ice extent at weekly to monthly scale between the Bering and Okhotsk Seas during the years 1972 to 1976, when northerly winds over the Bering Sea, which led to an increase in sea ice extent over the Bering Shelf and Aleutian Basin, were associated with easterly or southerly winds over the Okhotsk Sea, which effectively decreased sea ice extent there (Figure 6). During the last glacial period, the Bering Sea was a semi-enclosed basin similar to the present Okhotsk Sea, and should have experienced increased extents of seasonal sea ice [e.g., *Sancetta and Robinson*, 1983; *Katsuki and Takahashi*, 2005]. Moreover, a prevalence of northerly winds has been suggested for the LGM based on loess deposits in Alaska [*Muhs et al.*, 2003]. Hence, if northerly winds were dominant over the Bering Sea during cold periods such as Heinrich events in analogy with modern cold winters and the LGM, intense brine rejection and associated intermediate or deep water ventilation would have occurred around potentially widespread areas of polynya over the northeastern part of the Aleutian Basin.

9.5. Calm Realm With High Productivity in the Bering and Okhotsk Seas During Interstadials and the Bølling/Allerød Period

[51] Primary productivity at the northeastern slope of the Bering Sea appears to have drastically increased during periods, which we suggest to correspond to DOIS between ~50 and ~35 ka, based on prominent peaks of $\%CaCO_3$, generally increased biogenic silica contents [*Itaki et al.*, 2009], and relatively low $\delta^{13}C_{bf}$. *Gorbarenko et al.* [2007] also found increased productivity during almost all DOIS of the last 80 kyr in the Okhotsk Sea based on bio-productivity indicators such as barium, organic carbon, carbonate, chlorine and the abundance of benthic foraminifera. These high productivity events in both the Bering and Okhotsk Seas were possibly associated with decreases in NPIW formation in the Bering Sea, which are suggested by the occurrence of warmer and/or less saline, and possibly less oxygenated (consequently more nutrient-enriched) intermediate waters on the northeastern Bering Sea slope. Also the

general absence of lateral advection between the Bering and Okhotsk Seas based on similar values in $\delta^{18}O_{bf}$ at intermediate depth during those periods implies that calm and rather stratified intermediate to surface water conditions should have prevailed in the two seas.

[52] The B/A period was oceanographically unique, because the sedimentary record shows occurrence of widespread laminated sediments at intermediate water depths around the North Pacific continental margins [e.g., *Cannariato and Kennett*, 1999; *Zheng et al.*, 2000; *van Geen et al.*, 2003; *Cook et al.*, 2005; *Hendy and Pedersen*, 2005; *Ikehara et al.*, 2006]. Whether this marked period of low intermediate water oxygen level was solely caused by high surface productivity [e.g., *Hendy et al.*, 2004; *McKay et al.*, 2005; *Dean*, 2007] or by additional decrease in ventilation of intermediate water [e.g., *Behl and Kennett*, 1996; *Cannariato and Kennett*, 1999; *Hendy and Pedersen*, 2005] has been widely discussed. Based on pore water oxygen and productivity indicators, *Hendy and Pedersen* [2005] observed low pore water oxygen contents during the Allerød accompanied by a decrease in the organic carbon rain rate, and increased pore water oxygen contents during YD, although the organic carbon rain rate remained at the same level as during the Allerød. They concluded that lateral advection of intermediate water derived from distal sources (i.e., northern sources [*Hendy and Pedersen*, 2006]) primarily drove changes in bottom water oxygen content at the California margin during deglaciation [*Kennett and Ingram*, 1995; *Behl and Kennett*, 1996; *Hendy and Kennett*, 2003; *Crusius et al.*, 2004]. Variable NPIW formation in the Bering Sea suggested in our study is consistent with this interpretation.

[53] As has been described before, the reduction in NPIW in the Bering Sea and deposition of laminated sediments during deglaciation at site MR06-04-23 apparently preceded the abrupt Bølling and earliest Holocene warming in Greenland by ~1 and ~0.5 kyr, respectively (Figure 5). These time leads significantly exceed the analytical calendar age uncertainties of ~70 to ~130 years (Table 1). We suggest that the time leads primarily reflect a temporal increase in the local surface water reservoir age to ~1700 years at the onset of the Bølling and ~1200 years at the onset of the earliest Holocene as a result of upwelling of old deep water that accumulated in the deeper part of the North Pacific during the LGM [*Galbraith et al.*, 2007; *Marchitto et al.*, 2007; *Sarnthein et al.*, 2007; *Tada et al.*, 2009]. These results are consistent with subarctic Pacific deep water ages of ~1900 years during H1 and ~1250 years during YD [*Galbraith et al.*, 2007], although these ages may be overestimated by a few hundred years due to temporarily increased reservoir ages (~1150 years) in the subarctic Pacific during deglaciation [*Sarnthein et al.*, 2007]. Although further research is needed to clarify the nature of these time leads, our results suggest that climate warming associated with the onset of the B/A period and the earliest Holocene would have temporarily interrupted formation of NPIW in the Bering Sea, giving way to nutrient-rich, and warmer and/or less saline North Pacific deep waters that upwelled at the Bering Sea continental slope [*Brunelle et al.*, 2007]. The ascension of this old and oxygen-poor water mass in the Bering Sea could have well increased the reservoir age of surface waters by several hundred years and led to the deposition of laminated sediments.

[54] Such shut-down of intermediate water formation in the Bering Sea during the B/A period might have also decreased oxygen levels along the western and eastern margins of the North Pacific beyond thresholds and caused the occasional deposition of laminated sediments [*Behl and Kennett*, 1996; *van Geen et al.*, 2003; *Crusius et al.*, 2004; *Hendy and Pedersen*, 2005], directly through decreased lateral advection of oxygen-rich intermediate water and/or indirectly through increased consumption of dissolved oxygen in the intermediate water due to enhanced productivity caused by upwelling of nutrient-rich deep waters along the continental margin. Enhanced productivity along the North Pacific margins during the B/A period may have temporarily increased biological sequestration of CO_2, which is a possible mechanism to counteract large scale pCO_2 rise during deglaciation.

10. Summary and Conclusions

[55] We examined a possible link between D-O cycles and changes in intermediate water properties and surface productivity in the northeastern Bering Sea. Coeval positive excursions of $\delta^{18}O_{bf}$ and $\delta^{13}C_{bf}$, and low $\%CaCO_3$ in PC-23A suggest emergence of relatively cold and/or saline and possibly better oxygenated intermediate water at the northeastern Bering slope during periods of low surface productivity, which we tentatively correlated to H5, H4, H3, as well as several DOS during MIS 3, and to H1 and YD during the deglaciation. A comparison of $\delta^{18}O_{bf}$ between the central Okhotsk Sea and the Bering Sea indicates that intermediate water considerably cooled and/or became more saline in the Bering Sea during at least two cold periods of MIS 3, which we tentatively correlated to DOS 12 and H4, while such cooling and/or salinity increase was not evident in the central Okhotsk Sea during MIS 3.

[56] Furthermore, a comparison between ventilation changes off eastern Japan with gradients of $\delta^{18}O_{bf}$ between the Bering Sea and the southwestern Okhotsk Sea indicates that intermediate water was colder and/or more saline in the Bering Sea (higher $\delta^{18}O_{bf}$) than in the southwestern Okhotsk Sea (lower $\delta^{18}O_{bf}$) during H1 and YD, when the ventilation age off northeastern Japan significantly decreased. We accordingly propose that the Bering Sea was the probable source of NPIW during H1 and YD and possibly other severe cold periods of MIS 3, and that the cold and/or saline water mass may have occasionally spread southward at least to the area off Shimokita peninsula.

[57] During periods, which we correlated to DOIS and the B/A period, on the other hand, NPIW formation seems to have weakened (or ceased) both in the Bering and Okhotsk Seas, judging from the occurrence of warmer and/or less saline intermediate water at the Bering Sea slope and the absence of significant $\delta^{18}O_{bf}$ gradients between the Bering and Okhotsk Seas. These periods were also characterized by high surface productivity in both the Bering and Okhotsk Seas. Based on coeval occurrences of low $\delta^{18}O_{bf}$, low $\delta^{13}C_{bf}$ and high $\%CaCO_3$ in PC-23A, we suggest that a reduction or shutdown of ventilation in the Bering Sea during warm periods facilitated upward migration of aged, nutrient-rich waters from the deep North Pacific and thus promoted surface productivity in the northeastern Bering Sea. These processes could have also caused the temporal increase in

the marine reservoir age observed during the B/A period and the earliest Holocene. A reduction of ventilation during the B/A period in the Bering Sea may have been causally linked to sluggish ventilation off eastern Japan and could have contributed to generally low oxygen conditions at intermediate depths in the North Pacific at that time.

[58] An ultimate trigger for enhanced intermediate water production in the Bering Sea could have been predominantly northerly winds over the Bering Sea arising from an eastward shift of the Aleutian Low during severe cold periods, which should have created favorable conditions for active polynya formation and brine rejection in the northeastern Bering Sea. In the generally colder and dryer glacial environment, owing to greater continentality of the Bering Sea area [*Ager*, 2003; *Kurek et al.*, 2009], the resulting increase in sea surface salinity and density could have been sufficient for ventilating intermediate and/or deep waters. At the same time, such eastward shift of the Aleutian Low would have led to more easterly or southerly winds over the Okhotsk Sea that prevented polynya formation there and facilitated the introduction of relatively moist air from the North Pacific. These processes would have lowered sea surface salinity and effectively reduced intermediate water formation in the Okhotsk Sea during cold episodes of the last glacial period.

[59] **Acknowledgments.** We express our sincere thanks to the crew and onboard scientists of cruise MR06-04 for their assistance in sampling and sample preparation. We are thankful for assistance in picking planktonic foraminifera for ^{14}C analysis by K. Khim and S. Kim (Pusan University, South Korea). We are grateful for provision of modern bottom water oxygen isotope data at the studied core site by A. Ijiri. The comments of two anonymous reviewers greatly helped to improve the manuscript. This work is partly supported by grants-in-aid for scientific research from the Japan Society for Promotion of Science (18101001) to R.T. and by scholarships of the Ministry of Education, Science, Sports and Culture of Japan and the University of Tokyo to S.F.R.

References

Adkins, J. F., K. McIntyre, and D. P. Schrag (2002), The salinity, temperature and $\delta^{18}O$ of the Glacial Deep Ocean, *Science*, *298*, 1769–1773, doi:10.1126/science.1076252.

Ager, T. A. (2003), Late Quaternary vegetation and climate history of the central Bering land bridge from St. Michael Island, western Alaska, *Quat. Res.*, *60*(1), 19–32, doi:10.1016/S0033-5894(03)00068-1.

Ahagon, N., K. Ohkushi, M. Uchida, and T. Mishima (2003), Middepth circulation in the northwest Pacific during the last deglaciation: Evidence from foraminiferal radiocarbon ages, *Geophys. Res. Lett.*, *30*(21), 2097, doi:10.1029/2003GL018287.

Behl, R. J., and J. P. Kennett (1996), Brief interstadial events in the Santa Barbara Basin, NE Pacific, during the past 60 kyr, *Nature*, *379*, 243–246, doi:10.1038/379243a0.

Brunelle, B. G., D. M. Sigman, M. S. Cook, L. D. Keigwin, G. H. Haug, B. Plessen, G. Schettler, and S. L. Jaccard (2007), Evidence from diatom-bound nitrogen isotopes for Subarctic Pacific stratification during the last ice age and a link to North Pacific denitrification changes, *Paleoceanography*, *22*, PA1215, doi:10.1029/2005PA001205.

Cannariato, G., and J. P. Kennett (1999), Climatically related millennial-scale fluctuations in strength of California margin oxygen-minimum zone during the past 60 k.y, *Geology*, *27*(11), 975–978, doi:10.1130/0091-7613(1999)027<0975:CRMSFI>2.3.CO;2.

Cavalieri, D. J., and S. Martin (1994), The contribution of Alaskan, Siberian, and Canadian coastal polynyas to the cold halocline layer of the Arctic Ocean, *J. Geophys. Res.*, *99*(C9), 18,343–18,362, doi:10.1029/94JC01169.

Cavalieri, D. J., and C. L. Parkinson (1987), On the relationship between atmospheric circulation and the fluctuations in the sea ice extents of the Bering and Okhotsk seas, *J. Geophys. Res.*, *92*, 7141–7162, doi:10.1029/JC092iC07p07141.

Cook, M. S., L. D. Keigwin, and C. A. Sancetta (2005), The deglacial history of surface and intermediate water of the Bering Sea, *Deep Sea Res., Part II*, *52*, 2163–2173, doi:10.1016/j.dsr2.2005.07.004.

Cook, M. S., L. D. Keigwin, D. Birgel, and K.-U. Hinrichs (2011), Repeated pulses of vertical methane flux recorded in glacial sediments from the southeast Bering Sea, *Paleoceanography*, *26*, PA2210, doi:10.1029/2010PA001993.

Crusius, J., T. F. Pedersen, S. Kienast, L. Keigwin, and L. Labeyrie (2004), Influence of northwest Pacific productivity on north Pacific intermediate water oxygen concentrations during the Bølling-Ållerød interval (14.7–12.9 ka), *Geology*, *32*(7), 633–636, doi:10.1130/G20508.1.

Dean, W. E. (2007), Sediment geochemical records of productivity and oxygen depletion along the margin of western North America during the past 60,000 years: Teleconnections with Greenland Ice and the Cariaco Basin, *Quat. Sci. Rev.*, *26*(1–2), 98–114, doi:10.1016/j.quascirev.2006.08.006.

Dumond, D. E., and D. G. Griffin (2002), Measurements of the marine reservoir effect on radiocarbon ages in the eastern Bering Sea, *Arctic*, *55*(1), 77–86.

Duplessy, J. C., N. J. Shakleton, R. G. Fairbanks, L. Labeyrie, D. Oppo, and N. Kallel (1988), Deep water source variations during the last climatic cycle and their impact on the global deep water circulation, *Paleoceanography*, *3*, 343–360, doi:10.1029/PA003i003p00343.

Duplessy, J. C., M. Arnold, E. Bard, A. Juillet-Leclerc, N. Kallel, and L. Labeyrie (1989), AMS ^{14}C study of transient events and of the ventilation rate of the Pacific intermediate water during the last deglaciation, *Radiocarbon*, *31*, 493–502.

Dyke, A. S., J. T. Andrews, P. U. Clark, J. H. England, G. H. Miller, J. Shaw, and J. J. Veillette (2002), The Laurentide and Innuitian ice sheets during the Last Glacial Maximum, *Quat. Sci. Rev.*, *21*, 9–31, doi:10.1016/S0277-3791(01)00095-6.

Emile-Geay, J., M. A. Cane, N. Naik, R. Seager, A. C. Clement, and A. van Geen (2003), Warren revisited: Atmospheric freshwater fluxes and "Why is no deep water formed in the North Pacific," *J. Geophys. Res.*, *108*(C6), 3178, doi:10.1029/2001JC001058.

Epstein, S., S. R. Buchsbaum, H. A. Lowenstein, and H. C. Urey (1953), Revised carbonate-water isotopic temperature scale, *Geol. Soc. Am. Bull.*, *64*, 1315–1326, doi:10.1130/0016-7606(1953)64[1315:RCITS]2.0.CO;2.

Farrell, J. W., and W. L. Prell (1989), Climatic change and $CaCO_3$ preservation: An 800,000 year bathymetric reconstruction from the central equatorial Pacific Ocean, *Paleoceanography*, *4*, 447–466, doi:10.1029/PA004i004p00447.

Favorite, F., A. J. Dodimead, and K. Nasu (1976), Oceanography of the Subarctic Pacific Region, 1960–71, *Int. N. Pac. Fish. Comm. Bull. 33*, 187 pp.

Galbraith, E. D., S. L. Jaccard, T. F. Pedersen, D. M. Sigman, G. H. Haug, M. Cook, J. Southon, and R. Francois (2007), Carbon dioxide release from the North Pacific abyss during the last deglaciation, *Nature*, *449*, 890–893, doi:10.1038/nature06227.

Gorbarenko, S. A., I. A. Basov, M. P. Chekhovskaya, J. Southon, T. A. Khusid, and A. V. Artemova (2005), Orbital and millennium scale environmental changes in the southern Bering Sea during the last glacial-Holocene: Geochemical and paleontological evidence, *Deep Sea Res., Part II*, *52*, 2174–2185, doi:10.1016/j.dsr2.2005.08.005.

Gorbarenko, S. A., E. L. Goldberg, M. Kashgarian, T. A. Velivetskaya, S. P. Zakharkov, V. S. Pechnikov, A. A. Bosin, O. Y. Psheneva, and E. D. Ivanova (2007), Millennium scale environmental changes of the Okhotsk Sea during last 80 kyr and their phase relationship with global climate changes, *J. Oceanogr.*, *63*, 609–623, doi:10.1007/s10872-007-0054-1.

Graham, D. W., B. H. Corliss, M. L. Bender, and L. D. Keigwin (1981), Carbon and oxygen isotopic disequilibria of recent deep-sea benthic foraminifera, *Mar. Micropaleontol.*, *6*, 483–497, doi:10.1016/0377-8398(81)90018-9.

Haley, B. A., M. Frank, R. F. Spielhagen, and A. Eisenhauer (2008), Influence of brine formation on Arctic Ocean circulation over the past 15 million years, *Nat. Geosci.*, *1*(1), 68–72, doi:10.1038/ngeo.2007.5.

Hendy, I. L., and J. P. Kennett (2003), Tropical forcing of North Pacific intermediate water distribution during Late Quaternary rapid climate change?, *Quat. Sci. Rev.*, *22*, 673–689, doi:10.1016/S0277-3791(02)00186-5.

Hendy, I. L., and T. F. Pedersen (2005), Is pore water oxygen content decoupled from productivity on the California Margin? Trace element results from Ocean Drilling Program Hole 1017E, San Lucia slope, California, *Paleoceanography*, *20*, PA4026, doi:10.1029/2004PA001123.

Hendy, I. L., and T. F. Pedersen (2006), Oxygen minimum zone expansion in the eastern tropical North Pacific during deglaciation, *Geophys. Res. Lett.*, *33*, L20602, doi:10.1029/2006GL025975.

Hendy, I. L., T. F. Pedersen, J. P. Kennett, and R. Tada (2004), Intermittent existence of a southern California upwelling cell during submillennial climate change of the last 60 kyr, *Paleoceanography*, *19*, PA3007, doi:10.1029/2003PA000965.

Hood, D. W. (1983), The Bering Sea, in *Estuaries and Enclosed Seas*, edited by B. H. Ketchum, pp. 337–373, Elsevier Sci., Amsterdam.

Ijiri, A., Y. Kawada, A. Hirota, U. Tsunogai, F. Nakagawa, N. Harada, and T. Sakamoto (2009), Oxygen and hydrogen isotopic composition of the Bering Sea during the Last Glacial Maximum: Constraints from pore water analyses, *Eos Trans. AGU*, *90*(52), Fall. Meet. Suppl., Abstract PP13A-1383.

Ikehara, K., K. Ohkushi, A. Shibahara, and M. Hoshiba (2006), Change of bottom water conditions at intermediate depths of the Oyashio region, NW Pacific over the past 20,000 yrs, *Global Planet. Change*, *53*, 78–91, doi:10.1016/j.gloplacha.2006.01.011.

Ingle, J. C., Jr., et al. (1990), Section 2: Site reports, *Proc. Ocean Drill. Program, Initial Rep.*, *128*, 65–402.

Itaki, T., M. Uchida, S. Kim, H.-S. Shin, R. Tada, and B.-K. Khim (2009), Late Pleistocene stratigraphy and palaeoceanographic implications in northern Bering Sea slope sediments: Evidence from the radiolarian species Cycladophora davisiana, *J. Quat. Sci.*, *24*(8), 856–865, doi:10.1002/jqs.1356.

Katsuki, K., and K. Takahashi (2005), Diatoms as paleoenvironmental proxies for seasonal productivity sea-ice and surface circulation in the Bering Sea during the late Quaternary, *Deep Sea Res., Part II*, *52*, 2110–2130, doi:10.1016/j.dsr2.2005.07.001.

Katsuki, K., B.-K. Khim, T. Itaki, Y. Okazaki, K. Ikehara, Y. Shin, H. Yoon, and C. Y. Kang (2010), Sea-ice distribution and atmospheric pressure patterns in southwestern Okhotsk Sea since the Last Glacial Maximum, *Global Planet. Change*, *72*, 99–107, doi:10.1016/j.gloplacha.2009.12.005.

Keigwin, L. D. (1998), Glacial-age hydrography of the far Northwest Pacific Ocean, *Paleoceanography*, *13*(4), 323–339, doi:10.1029/98PA00874.

Keigwin, L. D., and G. A. Jones (1990), Deglacial climate oscillations in the Gulf of California, *Paleoceanography*, *5*, 1009–1023, doi:10.1029/PA005i006p01009.

Kennett, J. P., and L. Ingram (1995), A 20,000-year record of ocean circulation and climate change from the Santa Barbara basin, *Nature*, *377*, 510–514, doi:10.1038/377510a0.

Kennett, J. P., K. G. Cannariato, I. L. Hendy, and R. J. Behl (2000), Carbon isotopic evidence for methane hydrate instability during Quaternary interstadials, *Science*, *288*, 128–133, doi:10.1126/science.288.5463.128.

Kido, Y., T. Koshikawa, and R. Tada (2006), Rapid and quantitative major element analysis method for wet fine-grained sediments using an XRF microscanner, *Mar. Geol.*, *229*, 209–225, doi:10.1016/j.margeo.2006.03.002.

Kim, S.-J., and Y.-G. Park (2008), Glacial ocean circulation and property changes in the North Pacific, *Atmos. Ocean*, *46*(2), 257–275, doi:10.3137/ao.460205.

Kim, S., B.-K. Khim, T. Itaki, and H.-S. Shin (2008), Variation of calcium carbonate content and Dansgaard–Oeschger events in the continental slope of the central Bering Sea during the last 65 kyr [in Korean with English abstract], *Ocean Polar Res.*, *30*, 215–224, doi:10.4217/OPR.2008.30.3.215.

Koshikawa, T., Y. Kido, and R. Tada (2003), High-resolution rapid elemental analysis using an XRF microscanner, *J. Sediment. Res.*, *73*, 824–829, doi:10.1306/020503730824.

Kroopnick, P. M. (1985), The distribution of ^{13}C of ΣCO_2 in the world oceans, *Deep Sea Res., Part A*, *32*(1), 57–84, doi:10.1016/0198-0149(85)90017-2.

Kurek, J., L. C. Cwynar, T. A. Ager, M. B. Abbott, and M. E. Edwards (2009), Late Quaternary paleoclimate of western Alaska inferred from fossil chironomids and its relation to vegetation histories, *Quat. Sci. Rev.*, *28*, 799–811, doi:10.1016/j.quascirev.2008.12.001.

Kuzmin, Y. V., G. S. Burr, and A. J. T. Jull (2002), Radiocarbon reservoir correction ages in the Peter the Great Gulf, Sea of Japan, and eastern coast of the Kunashir, Southern Kuriles (Northwestern Pacific), *Radiocarbon*, *43*, 477–481.

Laj, C., C. Kissel, and J. Beer (2004), High resolution global paleointensity stack since 75 kyr (GLOPIS-75) calibrated to absolute values, in *Timescales of the Paleomagnetic Field*, *Geophys. Monogr. Ser.*, vol. 145, edited by J. E. T. Channell et al., pp. 255–265, AGU, Washington, D. C., doi:10.1029/145GM19.

Levitus, S., J. I. Antonov, T. P. Boyer, and C. Stephens (2000), Warming of the world ocean, *Science*, *287*, 2225–2229, doi:10.1126/science.287.5461.2225.

Lisiecki, L. E., and M. E. Raymo (2005), A Pliocene-Pleistocene stack of 57 globally distributed benthic $\delta^{18}O$ records, *Paleoceanography*, *20*, PA1003, doi:10.1029/2004PA001071.

Luchin, V. A., I. P. Semiletov, and G. E. Weller (2002), Changes in the Bering Sea region: Atmosphere–ice–water system in the second half of the twentieth century, *Prog. Oceanogr.*, *55*, 23–44, doi:10.1016/S0079-6611(02)00068-X.

Marchitto, T. M., S. J. Lehman, J. D. Ortiz, J. Fluckiger, and A. van Geen (2007), Marine radiocarbon evidence for the mechanism of deglacial atmospheric CO_2 rise, *Science*, *316*, 1456–1459, doi:10.1126/science.1138679.

Matsumoto, K., T. Oba, J. Lynch-Stieglitz, and H. Yamamoto (2002), Interior hydrography and circulation of the glacial Pacific Ocean, *Quat. Sci. Rev.*, *21*, 1693–1704, doi:10.1016/S0277-3791(01)00142-1.

McCorkle, D. C., L. D. Keigwin, B. H. Corliss, and S. R. Emerson (1990), The influence of microhabitats on the carbon isotopic composition of deep-sea benthic foraminifera, *Paleoceanography*, *5*(2), 161–185, doi:10.1029/PA005i002p00161.

McCorkle, D. C., H. Bruce, S. Corlis, and C. A. Farnham (1997), Vertical distributions and stable isotopic compositions of live (stained) benthic foraminifera from the North Carolina and California continental margins, *Deep Sea Res., Part I*, *44*(6), 983–1024, doi:10.1016/S0967-0637(97)00004-6.

McKay, J. L., T. F. Pedersen, and J. Southon (2005), Intensification of the oxygen minimum zone in the northeast Pacific off Vancouver Island during the last deglaciation: Ventilation and/or export production?, *Paleoceanography*, *20*, PA4002, doi:10.1029/2003PA000979.

McMillan, D. G., and C. G. Constable (2006), Limitations in correlation of regional relative geomagnetic paleointensity, *Geochem. Geophys. Geosyst.*, *7*, Q09009, doi:10.1029/2006GC001350.

Morley, J. J., and C. Nigrini (1995), Miocene to Pleistocene radiolarian biostratigraphy of North Pacific sites 881, 884, 885, 886, and 887, *Proc. Ocean Drill. Program, Sci. Results*, *145*, 55–91, doi:10.2973/odp.proc.sr.145.107.1995.

Muhs, D. R., T. A. Ager, E. A. Bettis III, J. McGeehin, J. M. Been, J. E. Begét, M. J. Pavich, T. W. Jr. Stafford, and D. S. P. Stevens (2003), Stratigraphy and paleoclimatic significance of late Quaternary loess-paleosol sequences of the last interglacial-glacial cycle in central Alaska, *Quat. Sci. Rev.*, *22*, 1947–1986, doi:10.1016/S0277-3791(03)00167-7.

North Greenland Ice Core Project Members (2004), High-resolution record of Northern Hemisphere climate extending into the last interglacial period, *Nature*, *431*, 147–151, doi:10.1038/nature02805.

Ohkushi, K., T. Itaki, and N. Nemoto (2003), Last glacial-Holocene change in intermediate water ventilation in the North Pacific, *Quat. Sci. Rev.*, *22*, 1477–1484, doi:10.1016/S0277-3791(03)00082-9.

Ohtani, K., Y. Akiba, and A. Y. Takenouti (1972), Formation of western subarctic water in the Bering Sea, in *Biological Oceanography of the Northern North Pacific Ocean*, edited by A. Y. Takenouti, pp. 32–44, Idemitsu Shoten Publ., Tokyo.

Okada, M., M. Takagi, and K. Takahashi (2005), Chronostratigraphy of sediment cores from the Bering Sea and the Subarctic Pacific based on paleomagnetic and oxygen isotopic analyses, *Deep Sea Res., Part II*, *52*, 2092–2109, doi:10.1016/j.dsr2.2005.08.004.

Okazaki, Y., K. Takahashi, H. Yoshitani, T. Nakatsuka, M. Ikehara, and M. Wakatsuchi (2003), Radiolarians under the seasonally sea-ice covered conditions in the Okhotsk Sea: Flux and their implications for paleoceanography, *Mar. Micropaleontol.*, *49*, 195–230, doi:10.1016/S0377-8398(03)00037-9.

Okazaki, Y., N. Harada, Y. Nakamura, and M. Sato (2008), Formation of the North Pacific Intermediate Water in the Okhotsk Sea after the last glaciations, paper presented at the 6th International Conference on Asian Marine Geology, Kochi Univ. of Technol., Kochi, Japan.

Okazaki, Y., A. Timmermann, L. Menviel, N. Harada, A. Abe-Ouchi, M. Chikamoto, A. Mouchet, and H. Asahi (2010), Deep water formation in the North Pacific during the Last Glacial termination, *Science*, *329*, 200–204, doi:10.1126/science.1190612.

Ortiz, J. D., S. E. O'Connell, J. DelViscio, W. Dean, J. D. Carriquiry, T. Marchitto, Y. Zheng, and A. van Geen (2004), Enhanced marine productivity off western North America during warm climate intervals of the past 52 kyr, *Geology*, *32*(6), 521–524, doi:10.1130/G20234.1.

Ostermann, D. R., and W. B. Curry (2000), Calibration of stable isotopic data: An enriched $\delta^{18}O$ standard used for source gas-mixing detection and correction, *Paleoceanography*, *15*(3), 353–360, doi:10.1029/1999PA000411.

Otsuki, A. S., S. Watanabe, and S. Tsunogai (2003), Adsorption of atmospheric CO_2 and its transport to the intermediate layer in the Okhotsk Sea, *J. Oceanogr.*, *59*, 709–717, doi:10.1023/B:JOCE.0000009599.94380.30.

Rahmstorf, S. (2002), Ocean circulation and climate during the past 120,000 years, *Nature*, *419*, 207–214, doi:10.1038/nature01090.

Reed, R. K., and P. J. Stabeno (1999), The Aleutian North Slope Current, in *Dynamics of the Bering Sea*, edited by T. R. Loughlin and K. Ohtani, pp. 177–191, Univ. of Alaska Sea Grant Press, Fairbanks, Alaska.

Reid, J. (1965), *Intermediate Waters of the Pacific Ocean*, *John Hopkins Oceanogr. Stud.*, vol. 2, 85 pp., John Hopkins Press, Baltimore, Md.

Reimer, P. J., et al. (2009), IntCal09 and Marine09 radiocarbon age calibration curves, 0–50,000 years cal BP, *Radiocarbon*, *51*, 1111–1150.

Robinson, S. W., and G. Thompson (1981), Radiocarbon corrections for marine shell dates with application to southern Pacific Northwest Coast prehistory, *Syesis*, *14*, 45–57.

Roden, G. I. (1995), Aleutian Basin of the Bering Sea: Thermohaline, oxygen, nutrient, and current structure in July 1993, *J. Geophys. Res.*, *100*(C7), 13,539–13,554, doi:10.1029/95JC01291.

Rodionov, S. N., N. A. Bond, and J. E. Overland (2007), The Aleutian Low, storm tracks, and winter climate variability in the Bering Sea, *Deep Sea Res., Part II*, *54*, 2560–2577, doi:10.1016/j.dsr2.2007.08.002.

Rogers, J. C. (1981), The North Pacific oscillation, *J. Climatol.*, *1*, 39–57, doi:10.1002/joc.3370010106.

Sakamoto, T., M. Ikehara, K. Aoki, K. Iijima, N. Kimura, T. Nakatsuka, and M. Wakatsuchi (2005), Ice-rafted debris (IRD)-based sea-ice expansion events during the past 100 kyrs in the Okhotsk Sea, *Deep Sea Res., Part II*, *52*, 2275–2301, doi:10.1016/j.dsr2.2005.08.007.

Sakamoto, T., et al. (2006), Millennial-scale variations of sea-ice expansion in the southwestern part of the Okhotsk Sea during the past 120 kyr: Age model and ice-rafted debris in IMAGES Core MD01–2412, *Global Planet. Change*, *53*, 58–77, doi:10.1016/j.gloplacha.2006.01.012.

Sancetta, C., and S. W. Robinson (1983), Diatom evidence on Wisconsin and Holocene events in the Bering Sea, *Quat. Res.*, *20*, 232–245, doi:10.1016/0033-5894(83)90079-0.

Sarnthein, M., et al. (2000), Fundamental modes and abrupt changes in North Atlantic circulation and climate over the last 60 ky – Concepts, reconstruction and numerical modeling, in *The Northern Atlantic: A Changing Environment*, edited by P. Schäfer et al., pp. 365–410, Springer, Berlin.

Sarnthein, M., P. M. Grootes, J. P. Kennett, and M.-J. Nadeau (2007), ^{14}C reservoir ages show deglacial changes in ocean currents and carbon cycle, in *Ocean Circulation: Mechanisms and Impacts—Past and Future Changes of Meridional Overturning*, *Geophys. Monogr. Ser*, vol. 173, edited by A. Schmittner, J. C. H. Chiang, and S. R. Hemming, pp. 175–196, AGU, Washington, D.C., doi:10.1029/173GM13.

Schrag, D. P., J. F. Adkins, K. McIntyre, J. L. Alexander, D. A. Hodell, C. D. Charles, and J. F. McManus (2002), The oxygen isotopic composition of seawater during the Last Glacial Maximum, *Quat. Sci. Rev.*, *21*, 331–342, doi:10.1016/S0277-3791(01)00110-X.

Schumacher, J. D., K. Aagaard, C. H. Pease, and R. B. Tripp (1983), Effects of a shelf polynya on flow and water properties in the northern Bering Sea, *J. Geophys. Res.*, *88*, 2723–2732, doi:10.1029/JC088iC05p02723.

Shackleton, N. J. (1974), Attainment of isotope equilibrium between ocean water and the benthonic foraminifera genus Uvigerina: Isotopic changes in the ocean during the last glacial, *Colloq. Int. CNRS*, *219*, 203–209.

Shcherbina, A. Y., L. D. Talley, and D. L. Rudnick (2003), Direct observations of North Pacific ventilation: Brine rejection in the Okhotsk Sea, *Science*, *302*, 1952–1955, doi:10.1126/science.1088692.

Singer, B. S., G. Hervé, B. R. Jicha, C. Laj, C. Kissel, B. L. Beard, and C. M. Johnson (2009), 40Ar/39Ar, K–Ar and 230Th–238U dating of the Laschamp excursion: A radioisotopic tiepoint for ice core and climate chronologies, *Earth Planet. Sci. Lett.*, *286*, 80–88, doi:10.1016/j.epsl.2009.06.030.

Springer, A. M., C. P. McRoy, and M. V. Flint (1996), The Bering Sea Green Belt: Shelf-edge processes and ecosystem production, *Fish. Oceanogr.*, *5*(3–4), 205–223, doi:10.1111/j.1365-2419.1996.tb00118.x.

Stuiver, M., and T. F. Braziunas (1993), Modeling atmospheric ^{14}C influences and radiocarbon ages of marine samples to 10,000 BC, *Radiocarbon*, *35*, 137–189.

Stuiver, M., and H. A. Polach (1977), Discussion: Reporting of ^{14}C data, *Radiocarbon*, *19*, 355–363.

Stuiver, M., and J. Reimer (1993), Extended ^{14}C data base and revised CALIB 3.0 ^{14}C age calibration program, *Radiocarbon*, *35*, 215–230.

Sverdrup, H. U., M. W. Johnson, and R. H. Fleming (1942), *The Oceans: Their Physics, Chemistry and General Biology*, Prentice-Hall, Englewood Cliffs, N. J.

Tada, R., S. Sato, T. Irino, H. Matsui, and J. P. Kennett (2000), Millennial-scale compositional variations in late Quaternary sediments at Site 1017, Southern California, *Proc. Ocean Drill. Program, Sci. Results*, *167*, 277–296, doi:10.2973/odp.proc.sr.167.222.2000.

Tada, R., S. Rella, M. Uchida, T. Itaki, K. Nagashima, and N. Harada (2009), Possible increase in reservoir age of the surface water in the northwestern Bering Sea during the deglacial period: Evidence of ascending aged North Pacific deepwater?, *Eos Trans. AGU*, *90*(52), Fall. Meet. Suppl., Abstract PP11E-07.

Takahashi, K. (2005), The Bering Sea and paleoceanography, *Deep Sea Res., Part II*, *52*, 2080–2091, doi:10.1016/j.dsr2.2005.08.003.

Talley, L. D. (1991), An Okhotsk Sea water anomaly: Implications for subthermocline ventilation in the North Pacific, *Deep Sea Res.*, *38*, 171–190.

Talley, L. D. (1993), Distribution and formation of North Pacific Intermediate Water, *J. Phys. Oceanogr.*, *23*, 517–537, doi:10.1175/1520-0485(1993)023<0517:DAFONP>2.0.CO;2.

Tanaka, S., and K. Takahashi (2005), Late Quaternary paleoceanographic changes in the Bering sea and the western subarctic Pacific based on radiolarian assemblage, *Deep Sea Res., Part II*, *52*, 2131–2149, doi:10.1016/j.dsr2.2005.07.002.

Uchida, M., Y. Shibata, M. Yoneda, T. Kobayashi, and M. Morita (2004), Technical progress in AMS microscale radiocarbon analysis, *Nucl. Instrum. Methods Phys. Res., Sect. B*, *223–224*, 313–317, doi:10.1016/j.nimb.2004.04.062.

Uchida, M., Y. Shibata, K. Ohkushi, M. Yoneda, K. Kawamura, and M. Morita (2005), Age discrepancy between molecular biomarkers and calcareous foraminifera isolated from the same horizons of Northwest Pacific sediments, *Chem. Geol.*, *218*, 73–89, doi:10.1016/j.chemgeo.2005.01.026.

Uchida, M., K. Ohkushi, K. Kimoto, F. Inagaki, T. Ishimura, U. Tsunogai, T. TuZino, and Y. Shibata (2008), Radiocarbon-based carbon source quantification of anomalous isotopic foraminifera in last glacial sediments in the western North Pacific, *Geochem. Geophys. Geosyst.*, *9*, Q04N14, doi:10.1029/2006GC001558.

van Geen, A., Y. Zheng, J. M. Bernhard, K. G. Cannariato, J. Carriquiry, W. E. Dean, B. W. Eakins, and J. Pike (2003), On the preservation of laminated sediments along the western margin of North America, *Paleoceanography*, *18*(4), 1098, doi:10.1029/2003PA000911.

Warner, M. J., and G. I. Roden (1995), Chlorofluorocarbon evidence for recent ventilation of the deep Bering Sea, *Nature*, *373*, 409–412, doi:10.1038/373409a0.

Warren, B. A. (1983), Why is no deep water formed in the North Pacific, *J. Mar. Res.*, *41*, 327–347, doi:10.1357/002224083788520207.

Watanabe, S., R. Tada, K. Ikehara, K. Fujine, and Y. Kido (2007), Sediment fabrics, oxygenation history, and circulation modes of Japan Sea during the Late Quaternary, *Palaeogeogr. Palaeoclimatol. Palaeoecol.*, *247*, 50–64, doi:10.1016/j.palaeo.2006.11.021.

Yasuda, I. (1997), The origin of the North Pacific Intermediate Water, *J. Geophys. Res.*, *102*(C1), 893–909, doi:10.1029/96JC02938.

Yokoyama, Y., K. Lambeck, P. de Deckker, P. Johnston, and L. K. Fifield (2000), Timing of the Last Glacial Maximum from observed sea-level minima, *Nature*, *406*, 713–716, doi:10.1038/35021035.

Yoshida, H., and N. Takahashi (1997), Chemical behavior of major and trace elements in the Horoman mantle diapir, Hidaka belt, Hokkaido, Japan, *J. Mineral. Petrol. Econ. Geol.*, *92*, 391–409, doi:10.2465/ganko.92.391.

Zahn, R., and A. C. Mix (1991), Benthic foraminiferal $\delta^{18}O$ in the ocean's temperature-salinity-density field: Constraints on ice age thermohaline circulation, *Paleoceanography*, *6*(1), 1–20, doi:10.1029/90PA01882.

Zheng, Y., A. van Geen, R. F. Anderson, J. V. Gardner, and W. E. Dean (2000), Intensification of the Northeast Pacific oxygen minimum zone during the Bölling-Alleröd warm period, *Paleoceanography*, *15*(5), 528–536, doi:10.1029/1999PA000473.